Chem Soc Rev

The structure and function of cell membranes examined with atomic force microscopy and single-molecule force spectroscopy

Journal:	*Chemical Society Reviews*
Manuscript ID:	CS-REV-12-2014-000508.R1
Article Type:	Review Article
Date Submitted by the Author:	18-Mar-2015
Complete List of Authors:	Shan, Yuping; Changchun Institute of Applied Chemistry, State Key Laboratory of Electroanalytical Chemistry Wang, Hongda; Changchun Institute of Applied Chemistry, State Key Laboratory of Electroanalytical Chemistry

The structure and function of cell membranes examined with atomic force microscopy and single-molecule force spectroscopy

Yuping Shan[1,2] and Hongda Wang[1,3,*]

[1]*State Key Laboratory of Electroanalytical Chemistry, Changchun Institute of Applied Chemistry, Chinese Academy of Sciences, Changchun, Jilin 130022, P.R. China.*
[2]*School of Chemistry and Life Science, Advanced Institute of Materials Science, Changchun University of Technology, Changchun 130012, P.R.China.*
[3]*Graduate University of Chinese Academy of Sciences, Beijing 100049, P.R. China.*

*Correspondence and requests for materials should be addressed to: H. D. Wang (hdwang@ciac.ac.cn)

Dr. Yuping Shan received her PhD in Changchun Institute of Applied Chemistry, Chinese Academy of Sciences in 2011, and then worked as a postdoctoral research associate in Department of Physics, Florida International University and Department of Chemistry and Biochemistry, University of South Carolina from 2012 to 2014. She is currently a faculty in Changchun University of Technology. The main interest of her research is the dynamic functions of cell membranes with single molecule force spectroscopy based on atomic force microscopy.

Professor Hongda Wang graduated from Department of Molecular Biology, Jilin University, P.R.China in 1995, BS. He received his PhD degree in 2000 from Changchun Institute of Applied Chemistry. Since the end of 2007, Dr. Wang worked as PI in Changchun Institute of Applied Chemistry, Chinese Academy of Sciences ("100 talent Program" of CAS). Dr. Wang was a visiting professor in Arizona State University in 2008. Dr. Wang's research interest is to study cell membranes by atomic force microscopy, molecular recognition imaging and super-resolution fluorescence microscopy. He has published more than 70 research papers in peer-reviewed journals.

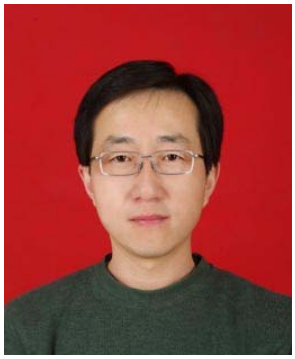

Abstract: The cell membrane is one of the most complicated biological complexes, and long-term fierce debates regarding the cell membrane persist because of technical hurdles. With the rapid development of nanotechnology and single-molecule techniques, our understanding of cell membranes has substantially increased. Atomic force microscopy (AFM) has provided several unprecedented advances (e.g., high resolution, three-dimensional and in situ measurements) in the study of cell membranes and has been used to systematically dissect the membrane structure in situ from both sides of membranes; as a result, novel models of cell membranes have recently been proposed. This review summarizes the new progress regarding membrane structure using in situ AFM and single-molecule force spectroscopy (SMFS), which may shed light on the study of the structure and functions of cell membranes.

1. Introduction

Cell membranes (or plasma membranes), the outermost layer of a cell, separate the cell from the environment.[1] Cell membranes are involved in various functions, such as the provision of a stable internal environment, transportation of substances between cells and the environment, energy conversion, and signal transduction.[2-4] The cell membrane is one of the most attractive topics for multidisciplinary studies, including studies that combine chemistry, biology and physics. For chemists, cell membranes are supermolecular structures that contain thousands of types of lipids, proteins and saccharides.[5] Biologists consider cell membranes to be the first barrier to defend cells from external harms, and cell membranes are related to multiple functions and diseases.[6] From a physicists' point of view, how the basic atoms and molecules can form a multi-functional and high-efficiency system is related to the origin of life.[7] After the basic structure (DNA and protein) was decrypted, scientists have paid more attention to the structure and function of whole supermolecular complexes, such as cell membranes and chromatin;[8-10] however, these studies are extremely challenging with our current technologies.

Cell membranes are large complexes that consist of vast lipids, saccharides and proteins (Figure 1).[11] Membrane lipids with both hydrophilic and hydropholic regions mainly include phosphoglycerides (e.g. dioleoyl phosphatidic acid, phosphatidic acid, phosphatidylcholine, phosphatidylethanolamine, phosphatidylserine, phosphatidylinositols), sphingolipids (ceramide, sphingomyelin, glycosphingolipid) and sterol lipids (e.g. cholesterol) (Figure 1a).[11] Membrane carbohydrates consist of

mannose, galactose, N-acetylglucosamine, glucose, fucose, N-acetylgalactosamine, sialic acid, and so on (Figure 1b).[12] Membrane proteins refer to transporters, receptors, enzymes and anchor proteins (Figure 1c).[11] In a cell, 25-40% of the proteins are associated with membranes;[13] membrane proteins, lipids and saccharides occupy approximately 50, 40 and 2-10%, respectively, of the mass of cell membranes.[1] Thousands of types of membrane proteins, lipids and saccharides have been characterized using proteomic and mass spectroscopy analyses.[14-15] However, where and how these elementary units (lipids, proteins and saccharides) are located in cell membranes have mainly remained unclear and controversial since the cell membranes were discovered.

Debates regarding the structure of cell membranes have a long history. Technical developments are always the basis of new understandings of cell membrane structure. Using simple extraction and Langmuir methods in 1925,[16] Gorter and Grendel extracted the lipid from a known number of erythrocytes and measured the lipid area, thereby concluding that the membrane consists of a double lipid layer. As a result, the famous term “lipid bilayer” was coined, which became a milestone in the study of membrane structure. To date, the location of proteins in the lipid bilayer has become a challenging and controversial topic regarding membrane structure.

After Cole and Harvey measured the surface tension of various cells,[17-18] Danielli and Davson proposed a sandwich membrane model (the Davson-Danielli model or the protein-lipid-protein model);[19] in this model, the lipid layer is covered by a protein layer on both sides. This model implies that the protein layer does not interact with the hydrophobic parts of the lipid bilayer and that the protein layer forms by simple physical adsorption. Because of the limits in the techniques 80 years ago, the Davson-Danielli model is not well supported by experimental data. With the development of electron microscopy (EM), more direct evidence regarding membranes was obtained in the 1950s. Sjöstrand et al. demonstrated that two dark bands were separated by a light band after staining with heavy metals.[20] Robertson subsequently interpreted the dark electron-dense bands as the lipid headgroups associated with protein layers [21] and proposed the “unit membrane” model (similar concept as the Davson-Danielli model), in which the lipid bilayer is located between two protein layers. Since then, the bilayer structure has been universally assigned to all membrane systems, including cell membranes and cellular organelle membranes. The Davson-Danielli model predominated until 1972, when Singer and Nicolson proposed the fluid mosaic model (FMM).[22]

With the development of the freeze-fracture technique and immuno-EM, researchers identified antibody-recognizing isolated membrane proteins and proteins

that spanned the lipid bilayer. Thus, Singer and Nicolson proposed the FMM with an isolated protein domain in the lipid bilayer in 1972 (Figure 2a);[22] this model emphasizes the fluidity of the membrane and the mosaic nature of proteins. The FMM positions the membrane proteins at appropriate locations (transmembrane), which is supported by experimental evidence (the freeze-fracture technique and immuno-EM). The FMM contributes to the dynamic features of cell membranes and has dominated to date.

However, because antibodies cannot detect the localization of all membrane proteins (immuno-EM only detects the separated proteins in the membrane), the FMM included a scheme in which monomeric membrane proteins randomly float in the sea of the lipid bilayer at low concentrations; the exposed hydrophobic side chains of these proteins span the lipid bilayer, and the bilayer surface is directly exposed to the aqueous environment. With additional evidence from protein structure, computer simulations and EM, Engelman updated the FMM to include more proteins in the membrane in 2005 (Figure 2b).[23]

The FMM successfully explains some characteristics, as indicated by the name of the model, of cell membranes, such as fluidity and protein mosaicism; however, it is not suitable to explain membrane functions, such as multiple protein-associated signal transduction and membrane endocytosis. With substantial evidence regarding protein clusters from biophysical studies (e.g., centrifugation, detergent extraction and cholesterol depletion by methyl-beta-cyclodextrin (MβCD)),[24] the lipid raft model (Figure 3 [25]), which implies that proteins exist in cholesterol-enriched domains to perform multiple functions (signal transduction, membrane trafficking), was proposed to interpret the multiple functions of transmembrane proteins in 1997.[26] The recent development of super-resolution imaging further confirmed the existence of lipid rafts.[27-28] However, the composition of lipid rafts and the interactions between multiple rafts remain far from clear. The statement “Do not study lipid rafts because they are uncertain” by some biophysicists represents the controversial state of lipid rafts.

The long history of cell membrane studies indicates that the membrane structure is far from completely understood. The major problem is the limitation of research approaches. Ex situ or indirect evidences were typically used to predict the structure of cell membranes. Therefore, high-resolution, in situ and direct observation techniques are highly desirable in the study of the whole membrane structure. In recent years, emerging single-molecule technologies (e.g., atomic force microscopy (AFM), single-molecule force spectroscopy (SMFS), and single-molecule fluorescence microscopy [29-32]) have provided an unprecedented opportunity to study

the structure of cell membranes at the single-molecule level.

AFM has been widely used in the study of biological samples.[33-34] With a nanometer resolution, AFM can provide three-dimensional structural information regarding biomacromolecules at the single-molecule level.[35] The sample preparation for AFM is relatively simple without complicated processing. AFM imaging of biological samples in liquid environments (especially combined with in situ enzymology) provides dynamic information regarding biological molecules under nearly physiological conditions.[36] These advantages have made AFM a powerful tool in cell biology (Table 1).[37] In addition, SMFS is a highly sensitive method to measure intermolecular forces down to the piconewton level.[38-40] In this review, we will summarize the progress of AFM and SMFS in the study of the structure and function of cell membranes at the single-molecule level, and novel models for the study of cell membranes will be discussed.

2. Principle of AFM and related techniques

2.1 AFM

AFM, which was invented in 1986 by Binnig et al.,[41] is an important member of the family of scanning probe microscopy techniques and provides molecular-scale imaging of non-conducting materials. In contrast to optical microscopy and EM, AFM overcomes the wavelength limit of to provide images of samples in various environments (vacuum, atmosphere, and liquid) with three-dimensional topography.[42-43] The lateral and vertical resolutions of AFM reach 1 nm and 0.1 nm, respectively.[44] AFM has been used in various areas of science and technology with excellent results.

The setup and working principle of AFM is shown in Figure 4; a sample is imaged using a tiny tip on a cantilever that detects the weak interactions between the tip and the sample surface. As the probe approaches the specimen surface, the attraction force from the interaction between the sample and the tip induces either a deflection of the cantilever probe (contact mode) or an amplitude change (tapping mode). A photodetector detects the shift or amplitude change and converts this signal to an electrical signal read by a computer; as a result, the surface information is recorded. The imaging modes of AFM are divided into the following major categories according to whether the tip contacts the sample: the contact mode AFM, tapping mode AFM (or MAC mode), and non-contact AFM mode.[45]

The contact mode was developed first, has the highest resolution, and is a commonly used AFM mode.[46] In this mode, the AFM tip contacts the sample surface

and is scanned using a piezoscanner. The contact mode is able to obtain high resolution images in both air and liquid. However, because of the existence of surface shear stress, this mode may deform soft samples; thus, it is not ideal for imaging unstable and flexible samples. The tapping mode pioneered by Hansma's group uses a constant driving force (acoustic, magnetic) to vibrate the cantilever at a certain frequency.[47-49] The resolution of the tapping mode AFM is similar to the contact mode AFM. The advantage of the tapping mode AFM is the short contact time and the minimum contact force, which effectively prevents damage to the samples from tip scanning. The tapping mode AFM (or dynamic force microscopy, MAC mode) in liquid is often used to image live biological samples (such as cells and bacteria) and to monitor the progress of reactions in solution.[50] In non-contact mode, there is a certain distance between the tip and the sample surface (typically a few nanometers).[51] The AFM probe vibrates at its resonant frequency near the sample surface. Because there is no direct contact between the tip and the sample in the non-contact imaging mode, the tip does not destroy the sample surface during imaging, which makes this mode suitable for the observation of soft samples. However, when the sample surface is covered with a thin layer of water, the non-contact mode can only provide an image of the layer of water, which induces an image artifact. For samples with a rigid surface without an adsorbed layer, the non-contact, tapping and contact modes essentially provide similar topography information.

The comparisons of these three imaging modes clearly indicate that the tapping mode AFM (or MAC mode) prevents the shear force-induced destruction of samples that occurs in contact mode and overcomes the low resolution of the non-contact imaging mode. Therefore, with the advantages of high resolution and minimum destruction to the sample, the tapping mode (or MAC mode) is the most widely used AFM mode in biological fields.

2.2 Molecular recognition imaging (topography and recognition imaging (TREC)) based on AFM

AFM provides incomparable advantages for obtaining topography information regarding the surface of a sample. However, for a complex sample with multiple components, the height measurements of AFM are unable to differentiate between the species (e.g., for a mixture of two proteins, we cannot distinguish them from the shape and height). Molecular recognition imaging (TREC) is a technique for the identification of a particular molecule in a complex (Figure 5).[52-54] In principle, the AFM tip is functionalized with specific molecules (e.g., antibodies) to recognize the counterpart molecules on the surface (e.g., antigens). High-resolution topography and

recognition images are simultaneously obtained. As shown in Figure 5a, an AFM tip tethered to an antibody scans the surface; when there is a specific interaction between the sample and the antibody on the AFM tip, the amplitude of the AFM cantilever will be reduced, and feedback systems adjust the cantilever position (Δ) to maintain a constant amplitude. This peak change corresponds to the molecular recognition signal from the specific interactions. Molecular recognition imaging has excellent specificity and reproducibility, and it further expands the biological applications of AFM. AFM and molecular recognition imaging have excellent properties for the study of cell membrane structure. Recently, force-distance curve-based AFM has provided an alternative method for simultaneously obtaining high-resolution images and quantitative information regarding biological samples.[40, 55]

2.3 High-speed AFM

High-speed AFM is a rapidly growing technique because it can image a functional single molecule at video rate (30-60 ms/frame).[56-58] Ando et al. successfully developed high-speed AFM for biological imaging and demonstrated the high potential for applications in biomolecular dynamics.[57, 59] With small cantilevers and a sensitive optical beam deflection (OBD) detector, high-speed AFM visualizes the movement of a single myosin molecule (V-shape) on actin filaments (Figure 6).[60] Cell membrane activities (cellular filopodia and membrane network structure) have been visualized using high-speed AFM.[61] Scheuring et al. visualized the movement of the aquaporin-O array and single proteins in the cell membrane of eye lens cells.[62] Combined with fluorescence microscopy, high-speed AFM provides the opportunity to identify dynamic processes of the cell membrane in living cells.[61] Further reviews regarding high-speed AFM are provided in the references.[57, 63]

2.4 In situ imaging of biomolecules with alterable conditions using a fluid through liquid cell

In situ imaging is the greatest advantage of AFM compared with EM. To maintain biological samples in their native states, in situ imaging of cell membranes is desirable because a dry sample will be deformed and will not represent the physiological features. Environmental control can be realized using a fluid through liquid cell.[64-65] As shown in Figure 7, the use of a syringe to inject the appropriate solution from one end and remove the same volume solution from the other end can change the buffer conditions (e.g., the salt concentration and pH) during imaging, which is rather important to observe biomolecules at work. It is also important to maintain a constant solution volume and temperature during imaging because a small temperature change may cause drift between the cantilever AFM probe and the

sample, which thus affects repeated images in the same location. In liquid environments, high-resolution imaging of biological molecules and dynamic changes between individual molecules are important features for biologists. The fluid through liquid cell technique allows the real-time study of dynamic behaviors of single-molecule interactions.[64]

2.5 Single Molecule Force Spectroscopy (SMFS)

Force spectroscopy based on AFM is a powerful approach to study protein interactions and folding at the single-molecule level.[29-30, 66-67] The high sensitivity of a fine AFM cantilever allows detecting tens of piconewton forces,[68-69] which provides a unique opportunity to explore molecular interactions and dynamics under various environmental conditions. The force curve can be used to measure the interaction between biological molecules at the single-molecule level, such as molecular recognition between receptor and ligand, antibody and antigen, and complementary strands of DNA[70-73]. SMFS was also used to explore the intramolecular force; for instance, Gaub and Fernandaz probed the unique mechanical properties of single proteins and polysaccharides.[74-77] Figure 8 shows the typical process of obtaining an AFM force curve.[78] The approach (trace) and withdrawal (retrace) lines reflect the interactions between the sample and the AFM tip. When the tip approaches the surface, the attracting force can be detected; during withdrawal of the tip from the surface, the unbinding of two interacting target molecules (e.g., antibody-antigen, ligand-receptor) is detected. The slope of the force curve provides the sample characteristics (e.g., stiffness and deformation).[53, 79] In general, the force curve is used to extract information regarding the unbinding events. For a functional cell membrane (e.g., transportation and endocytosis), the advantage of force curves is the capability of studying a dynamic process by tracing the curve while the substance is transported via the cell membrane.

AFM-based force-volume mode can be used to map the local interaction force between molecules on an AFM tip and biological samples,[80-81] which thus provides an alternative method to map the surface characteristics. During imaging of the sample, the force curves are engaged at each contact point, and interaction information can be recorded using the force map.

2.6 Resolution of AFM for imaging biological samples

The lateral resolution of AFM is typically as small as a few nanometers, which is sufficient to distinguish single molecules. AFM can image the Y-shape of an antibody (approximately 10 nm) at single-molecule resolution.[82] With optimal sample preparation and imaging conditions, AFM has been used to achieve subnanometer

resolution (vertically: approximately 0.1 nm; laterally: approximately 0.6 nm [83]), which is extremely useful in the study of membrane structure. Using in situ AFM, Muller et al. studied the fine structure of the human communication channel protein connexin 26 in a dense protein array.[44] As shown in Figure 9, AFM clearly provides images of a hexamer structure of connexin 26. The Ca^{2+}-induced conformational change of the connexin can be visualized at a single-molecule resolution. Scheuring et al. published several studies that provided high-resolution information regarding patterned bacterial membranes (light harvesting complex proteins).[84] High resolution is easily obtained for the membrane protein from the pattern sample (e.g., the purple membrane) because of the stiff structure in the protein arrays.[85] Challenges remain for imaging native cell membranes because of the irregularity of the membrane proteins in a protein complex and the lack of a clear pattern in these membranes. Multifrequency force microscopy can optimize the AFM image and provide the potential to achieve high-resolution imaging of native cell membranes.[86]

3. Sample preparation of cell membranes

3.1 Substrate for membrane samples

Mica is an appropriate substrate for high-resolution AFM imaging because its surface is smooth at the atomic level. However, fresh mica surfaces are negatively charged, which is not suitable for the immobilization of negatively charged cell membranes. Silanization of mica by aminopropyltriethoxysilane (APTES) easily creates the positively charged surface; thus, membranes can be tightly attached on the surface for solution imaging. Briefly, after a desiccator is purged with argon for 2 min, 30 μL of APTES and 10 μL of *N*,*N*-diisopropylethylamine are each placed into small containers at the bottom of the desiccator.[64] The desiccator is subsequently purged with argon for an additional 2 min. Mica sheets are stripped using tape until the sheets are smooth and then placed in the desiccator. The desiccator is purged for an additional 3 min and then sealed off; the mica is exposed to APTES vapor for 1 h. After the APTES is removed, the treated mica (AP-mica) is stored in the sealed desiccator under argon.

Glass cover slips can be used for various cultured nucleated cells. Prior to cell culture, strict cleaning steps must be performed to obtain a smooth surface on the cover slips. In general, glass cover slips are cleaned using a detergent and sonicated in 1 M potassium hydroxide for 20 min at room temperature. The cover slips are rinsed with Milli-Q water and subsequently stored in absolute ethyl alcohol. Prior to use, the glass sides and cover slips are washed three times with sterile distilled water and dried

with pure argon. The clean cover slips are placed in a culture dish as the substrate for cells.[87]

To study membrane functions and properties in situ, two-chamber substrates based on silicon or a porous silicon membrane were designed.[88-90] Scheuring et al. used electron beam lithography to prepare nano-hole arrays in Si(001) [88] (Figure 10). A two-chamber cell was used as the substrate in an S-layer study that also used fluorescence microscopy. William et al. fabricated a porous silicon membrane on the chamber,[89] in which the buffer solution was easily changed during AFM imaging.

3.2 Preparation of red blood cell membranes

There are several methods to prepare membranes, such as the method of shearing open red blood cells and the hypotonic lysis-centrifugation method. The shearing open method is appropriate for the preparation of a clean membrane with minimum damage (Figure 11).[91] The following simple steps are used: [92] two drops of blood are taken from a fingertip and centrifuged in 1 mL of PBS buffer (136.9 mmol/L NaCl, 2.7 mmol/L KCl, 1.5 mmol/L KH_2PO_4 and 8.1 mmol/L $Na_2HPO_4{\cdot}7H_2O$, pH 7.4) 5 times (1000 rpm for 2 min). A 100 μL drop of red blood cells in PBS buffer is subsequently deposited on the mica surface for approximately 20 min of absorption. Next, PBS is used to wash out the non-adsorbed cells. As shown in Figure 11a, a syringe is adjusted to obtain a 20° angle to the sample surface, and 10 mL of hypotonic buffer (6.85 mmol/L NaCl, 0.135 mmol/L KCl, 0.075 mmol/L KH_2PO_4, and 0.405 mmol/L $Na_2HPO_4{\cdot}7H_2O$, pH 7.4) is injected to flush the mica surface and obtain a flat membrane patch.

Using the hypotonic lysis-centrifugation method, the whole erythrocyte ghost membranes can be prepared as follows.[93] Briefly, erythrocytes are collected and cleaned by centrifugation in physiological buffer solution. The cells are lysed using a low-salt buffer (5 mM Na_3PO_4/Na_2HPO_4) and washed several times by centrifugation at 20,000 g for 20 min at 0°C until the ghost pellet becomes white. The membrane pellet is diluted in buffer for deposition on a coverslip or mica.

3.3 Preparation of the cytoplasmic side of membranes

The cell membranes are prepared by the shearing open method.[94] Briefly, the cells are washed twice with buffer (20 mM PIPES, 150 mM KCl, pH 6.2) on ice, incubated with ice-cold hypotonic buffer (4 mM PIPES and 30 mM KCl, pH 6.2) for 3 min, and then sheared open by a stream of 10 mL of hypotonic buffer through a needle at an angle of 20°. The membranes are subsequently treated with high-salt buffer (2 M NaCl, 1.5 mM KH_2PO_4, 2.7 mM KCl, and 1 mM Na_2HPO_4, pH 7.2) for 30 min at

room temperature to remove the cytoskeletons. The prepared membranes are immediately imaged in buffer using AFM. Ultrasonic stimulation is an alternative method for the preparation of the cytoplasmic side of membranes, as shown in Figure 12.[95] The inside-out membrane on the substrate is washed using buffer for AFM imaging.

The apical cytoplasmic side of membranes can be prepared by stripping the membrane from the top of a cell.[96-97] Briefly, the cells are cultured on glass slides (Figure 13). A poly-L-lysine-coated coverslip is lightly pushed on the cells, and the coverslip is then detached to obtain the top layer of the cell membranes. After the surface is rinsed using buffer solution, the cytoplasmic side of membranes can be imaged using AFM.

3.4 Preparation of the ectoplasmic side of membranes

Two strategies are used to prepare the ectoplasmic side of membranes. First, the ectoplasmic side of membranes can be imaged at the flat edge of a living cell under native conditions. Second, the ectoplasmic side of membranes can be obtained using the hypotonic lysis-centrifugation method.[94] Briefly, cells are first incubated with nocodazole (60 μM) and cytochalasin B (20 μM) for 50 min at 37°C to destroy the actin filaments and microtubules; the cells are subsequently digested using trypsin (1 mg/mL) and washed with 1 mL of PBS (136.9 mM NaCl, 2.7 mM KCl, 1.5 mM KH_2PO_4, and 8.1 mM $Na_2HPO_4 \cdot 7H_2O$, pH 7.4) three times. The cells are treated with 1 mg/mL DNase to digest the nuclei/DNA and then centrifuged at 3000 rpm for 10 min. The membrane precipitate is dissolved in PBS and deposited on APTES-mica for AFM imaging.

3.5 Preparation of large oocyte membranes

The membranes of large oocytes can be prepared using several methods, such as pipette manipulation and centrifugation.[98-99] A glass capillary pipette can be used to manipulate a whole *Xenopus laevis* oocyte. The oocyte is easily burst by exposing it to the air-water interface. Clean membranes without cytosolic contents are deposited on freshly cleaved mica for AFM imaging.[98] The attachment of oocytes onto a poly-L-lysine-coated glass substrate is also a convenient approach to peel off oocyte membranes for stable AFM imaging.[91]

It is worth noting that to obtain the native structure of cell membranes without damage, it is not recommended to fix the membrane using chemicals (e.g., glutaraldehyde) because they may crosslink the membrane proteins and result in local destruction of the membranes (e.g., blurred images because of protein cross-linking).[100]

3.6 Preparation of an artificial lipid bilayer

The evaporation method is an appropriate method to prepare an artificial lipid bilayer.[101] Briefly, a mixture of lipids is solubilized in an organic solvent. After evaporation of the solvent under nitrogen, the lipids are dried by desiccation under a vacuum. The dried lipid film is subsequently resuspended in an aqueous buffer solution, which yields a suspension of multilamellar vesicles. These multilamellar vesicles can be further treated by sonication or extrusion to obtain small unilamellar vesicles or large unilamellar vesicles. Artificial lipid bilayers are formed on a solid substrate by depositing these suspensions of vesicles onto freshly cleaved mica.

By an electroformation method, giant unilamellar vesicles were produced by Schwille et al.[102-103] Briefly, a perfusion chamber was equipped with two glass slides coated with conductive indium tin oxide (ITO). Lipids in chloroform/methanol 9:1 (5 mM, under a nitrogen atmosphere) were deposited on preheated ITO slides and the solvent was evaporated at 20 or 60 °C. After adding water into the chamber, a voltage of 1.1 V at 10 Hz was applied for 1 h. After lipid swelling, the chamber was cooled down slowly by a heat block. The prepared vesicles can be deposited on mica for AFM imaging. In addition, Langmuir-Blodgett method is a traditional approach to prepare the supported lipid bilayers; detailed methods can be found in references.[104-106]

4. Examination of the structure of cell membranes by AFM

4.1 Examination of model membranes (artificial membranes)

As a result of the complexity of structure and function, the study of native cell membranes is difficult. Therefore, researchers first used artificial membranes to mimic the cell membrane.[107] Under near physiological conditions, AFM can indicate the nano-structures and mechanical properties of artificial membranes, the functions of biomembranes and the interactions between membranes and nano-particles. Using AFM, Morandat et al. explored the nano-structured information of artificial lipid bilayer membranes composed of dioleoylphosphatidylcholine/ dipalmitoylphosphatidylcholine (DOPC/DPPC) and the effect of Triton X-100 on these membranes (Figure 14).[108] The addition of a cholesterol molecule to the SLBs significantly increased the resistance of the bilayer to Triton X-100, which confirms cholesterol molecules play a key role in the detergent resistance of membranes.[109] Moreover, with the addition of 1% ganglioside GM1 into SLBs to mimic the composition of lipid rafts in cell membranes, an AFM study demonstrated that GM ganglioside leads to the formation of ganglioside-rich microdomains (40-100 nm).[110]

Because artificial membranes have a definite composition, a membrane protein (e.g., KcsA potassium channel) can be inserted into the lipid bilayer to visualize the dynamic conformation of the membrane protein (channel opening and closing) at high resolution.[111] Although some characteristics of cell membranes can be deduced using a model membrane (e.g., phase separation and raft domains enriched with cholesterol), this model is still too simple to explain the native membrane behavior because there are many lipids and proteins in cell membranes and because the interactions between them are sophisticated.

4.2 Examination of functional microdomains in cell membranes

Since the proposal of the FMM of cell membranes in 1972, some phenomena regarding cell membranes have been interpreted appropriately, such as the mosaic proteins and fluidic cell membranes. However, this model cannot explain complicated membrane functions. The lipid raft model focuses on functional microdomains enriched with cholesterol, sphingomyelin, and membrane proteins.[26, 112] Many cellular functions are associated with lipid rafts, such as signal transduction, protein-mediated endocytosis and viral infection.[113-114] Lipid rafts are dynamic and polymorphous; thus, conventional methods are not suitable for their studies. In general, the size of lipid rafts is considered to be in the range of several hundred nanometers. Traditional methods, such as sucrose density gradient centrifugation, electrophoresis, fluorescence staining and EM, are likely to damage the structure of lipid rafts. Fluorescence microscopy studies provided solid contributions to the understanding of lipid rafts[115]; in particular, super-resolution imaging demonstrated the dynamic characteristic of lipid rafts.[27] However, Shaw et al. determined that only visualizing membrane domains using a fluorescent probe may induce artifacts.[116-117] AFM provides features of the absolute topography of lipid rafts. Because of the high resolution and the in situ and alterable imaging conditions, AFM has high potential to resolve the unanswered questions regarding lipid rafts.

Phase separation according to the type of lipid was confirmed using a model lipid bilayer (supported DOPC/DPPC bilayer), in which an AFM image indicated that lipids enriched with cholesterol tend to form domains resistant to Triton X-100.[109] Orsini et al. used sucrose-density gradient centrifugation to isolate lipid raft domains from Triton X-100 treated cells and AFM to directly confirm that there are lipid rafts associated with specific proteins in membranes.[118] However, the whole cell lysis may induce contamination from the endomembrane system (e.g., Golgi and endoplasmic reticulum). In situ treatments and observations of cell membranes are highly desirable for these studies.

Lipid rafts exist in most membrane systems, such as erythrocytes, nucleated cells and plant cells.[27, 119-120] In red blood cell membranes, detergent-resistant membrane (DRM) domains were first confirmed using in situ imaging, which exhibited an irregular shape with a size of several hundred nanometers (Figure 15a-c).[119] The in situ observation of the specific extraction of cholesterol (a key component in lipid rafts) by MβCD has provided convincing results. As shown in Figure 15d-g, in-situ AFM demonstrated that MβCD gradually eroded the membrane with time. The size of the eroded irregular patches is mainly in the range of 100-300 nm. Unlike the living cell, the cell membrane was electrostatically absorbed on the APTES-mica for AFM imaging, thus the lipid rafts can be stably imaged by AFM for long time.[119] Additional evidence has indicated that lipid rafts exist in nucleated cell membranes. Chen et al. detected the depletion of lipid rafts from endothelial cells by MβCD using AFM and fluorescence microscopy.[121] The lipid raft is the functional unit and is associated with the underlying cytoskeletal network for the control of dynamic functions,[122] as confirmed by AFM force measurements.[123]

4.3 The structure of red blood cell membranes

4.3.1 Imaging membrane proteins on the cytoplasmic side of native membranes

The advantage of AFM is the capability to image the whole cell membrane at high resolution under physiological conditions.[81, 124-125] The red blood cell is simple and is traditionally used as a model to study cell membranes. Many membrane proteins are located in real cell membranes, and the determination of protein distribution is the major goal in the study of cell membrane structure. The whole inner membrane of red blood cells is simply prepared using a shearing open method. In Figure 16a, dense membrane proteins and a rough inner membrane surface (the average roughness is approximately 1.9 nm) are observed, which supports the view of Engelman that suggests “more mosaic than liquid”.[92] Fluorescence and super-resolution imaging subsequently demonstrated that these proteins exist in protein clusters (or lipid rafts).[28, 87, 126-127] The height of cell membranes is approximately 10 nm, and the lipid bilayer is approximately 2.94 ± 0.36 nm; these results are consistent with other measurements.[128] Inner transmembrane proteins can be digested using enzymes, and this process clearly demonstrates the relative positions of the lipid bilayer and membrane proteins (i.e., the proteins sit on the lipid bilayer, and the lipid bilayer closely contacts the mica substrate) (Figure 16b).

To position particular proteins in the membrane, the TREC technique is a unique approach for the identification of proteins in a membrane complex using the corresponding antibody.[129] Figure 16c shows that the protein domain was recognized

by anti-ATPase.[130] The Na^+ K^+-ATPase molecules are dispersed and located in the membrane within a cluster in the recognized area. Using the same technique, Schillers et al. identified the cystic fibrosis transmembrane conductance regulator (CFTR, a protein of the adenosine triphosphate-binding cassette transporter superfamily) in the cell membranes of red blood cells.[131]

4.3.2 Imaging the outer surface of a red blood cell

The ectoplasmic side of red blood cell membranes is a mystery and as a default, it has been considered to be the same as the cytoplasmic side. Recently, AFM provided a complete picture of the outer surface in situ.[92] Interestingly, the outer membrane clearly demonstrates the opposite result compared with the inner surface. Although the AFM z resolution reaches down to 0.1 nm, a smooth outer surface without obvious protein protrusions has been observed (the roughness of the outer membrane is approximately 0.2 nm, which is 10 times less than the inner membrane). These findings suggest that the membrane protein distribution is much more asymmetrical than previously proposed. By TREC imaging, the saccharides (mannose) have been located by MNA-M lectin, which confirms that the mannose tends to form clusters (Figure 16e). The membrane saccharides are further located in the middle of lipid heads verified by the digestion with the saccharide enzyme (Figure 16f).

Caution is required when imaging the outer membrane because the sharp AFM cantilever can destroy the relatively soft outer lipid bilayer membrane and induce imaging artifacts. Tapping mode (or MAC mode) in solution and a regular tip radius (approximately 20 nm) are better for imaging a soft lipid bilayer. In addition, the use of glutaraldehyde to fix a cell may cause crosslinking of membrane proteins and produce artifacts in the membrane appearance.[100, 132]

4.3.3 New model of red blood cells – the semi-mosaic Model

From AFM observations, Wang et al. proposed the semi-mosaic model for the red blood cell membrane (Figure 16g); this model suggests that proteins may be partly set within the lipid bilayer rather than protruding out of the outer cell surface.[92] The saccharides are located in the middle of lipid hydrophilic heads, and the membrane proteins are mainly located on the cytoplasmic side of membranes. STORM imaging suggests that membrane proteins tend to form clusters in cholesterol-enriched domains (or lipid rafts).[87] To clarify whether the asymmetric structure of red blood cells is a common structure, Wang et al. also studied other red blood cell membranes in an evolutionary order from lower vertebrates (fish), reptiles (turtle) to birds (chicken), and the researchers determined that the features of these membranes are

very similar to human red blood cell membranes, with the exception of the size and nuclei (Table 2).[133-135]

4.4 Examination of nucleated mammalian cell membranes by AFM

4.4.1 The cytoplasmic membrane of nucleated mammalian cells

Similar to the situation in red blood cell membranes, many membrane proteins are exposed on the cytoplasmic side of nucleated mammalian cell membranes. An AFM topography image of South African frog oocyte membranes indicated protein particles with sizes of hundreds of nanometers, which is larger than a single protein, and suggests the membrane proteins form clusters that contain multiple proteins (Figure 17).[91] Functional structures (e.g., clathrin pits) perform the dynamic functions required for membrane transportation. Usukura et al. provided direct evidence of the existence of clathrin pits on the cytoplasmic side of cell membranes using high-resolution AFM imaging (Figure 18).[95] The same type of membrane protein is randomly distributed in the inner membrane; this distribution was verified via the use of labeled quantum dots to locate prestin (a membrane protein) in the inner membrane of CHO cells.[136] The pattern of membrane proteins in the inner membrane is closely associated with membrane activity. Vijayan et al. studied the changes in membrane proteins in response to an acute stress that induced the stress signaling pathways, and the researchers demonstrated that the protein domains became larger after stressor exposure [137]. Using fluorescence imaging, Burns et al. located multiple membrane components (including immunoglobulin E receptors, cholera toxin-aggregated GM1 and clathrin) and suggested that cholesterol-enriched domains (lipid rafts) are responsible for signaling and endocytosis.[96]

Enzyme digestion (trypsin or proteinase K) and solvent treatment (Triton X-100 or MβCD) during AFM imaging are appropriates methods for the dissection of the membrane architecture. The digested membrane exhibits a smooth surface with a height of 8 nm (Figure 19a and 19c).[94] After further treatment with Triton X-100, an outer protein layer that was approximately 4 nm thick was observed (Figure 19b), which confirms the digested membrane consists of a lipid bilayer (4 nm) and an outer protein layer (4 nm).

4.4.2 The ectoplasmic side of nucleated mammalian cell membranes

Because complicated cell membranes have more functions (e.g., signaling transduction and membrane transporting), the ectoplasmic side of nucleated mammalian cell membranes exhibit more proteins (e.g., receptors) on the surface. Using the TREC technique, Van Vliet et al. mapped vascular endothelial growth

factor receptor-2 (Figure 20),[54] which indicated an irregular distribution of the receptors in the membrane. Tang et al. located the human gonadotropin-releasing hormone receptor using TREC [138] and concluded that the receptor tends to form domains.

Without chemical fixation, in situ AFM demonstrated that the outer surface of complicated cell membranes has a roughness of 1.1 ± 0.2 nm (Figure 19f), which is quite different from the inner membrane. The dense protein layer that covers the lipid bilayer has been verified by enzyme digestion and in situ AFM imaging. After digestion with proteinase K, the protein layer is removed (Figure 19g). Further treatment with MβCD has suggested that the lipid bilayer lies underneath the dense protein layer (Figure 19h). The relationship between the protein layer and the lipid bilayer was further confirmed by digestion with a more specific enzyme (collagenase 3) (Figure 19i-k). The dense protein layer may consist of GPI protein, matrix protein and the ectoplasmic parts of transmembrane proteins (e.g., receptors).

4.4.3 New model of nucleated mammalian cell membranes - protein layer-lipid-protein island (PLLPI)

Although current cell membrane models (e.g., liquid mosaic model) tend to assign the same structure to all membranes from different cells, there is definitely a substantial difference between red blood cells and nucleated body cells. For example, the functions of nucleated mammalian cell membranes are substantially more complicated compared with human red blood cell membranes (almost no interaction with other cells and only carrying oxygen); thus, there are more receptors in their membranes compared with red blood cells. Combining in situ AFM imaging with enzyme digestion in fluid through liquid cell,[94] Wang et al. studied various mammalian cell membranes and demonstrated the following: the proteins on the ectoplasmic side of the cell membrane form a dense protein layer (~ 4 nm) on top of a lipid bilayer; proteins aggregate to form islands that are evenly dispersed on the cytoplasmic side of the cell membrane with a height of approximately 10-12 nm (a structural pattern similar to the inner cell membrane can be observed in large oocytes [98]); cholesterol-enriched domains exist within the cell membrane; carbohydrates remain in microdomains on the ectoplasmic side; and exposed amino groups are asymmetrically distributed on both sides. On the basis of these observations, Wang et al. proposed a PLLPI model for mammalian nucleated cell membranes, as shown in Figure 21. The PLLPI model emphasizes that the dense protein layer is the main functional component in the membrane in terms of mechanical properties, signaling transduction and material transport. A protein domain could be observed on the inner

side of cell membranes, which may function as functional clusters (i.e., lipid rafts). It is worth noting that the PLLPI model is only for a static and basic cell membrane that lacks cell-cell interactions. In tissue, membrane proteins could tend to protrude out of the membrane surface to interact with the cell matrix.[139]

The thickness of various membranes is shown in Table 2. The proposed "semi-mosaic" model for red blood cell membranes and the PLLPI model for nucleated mammalian membranes clearly indicate the universality of membrane asymmetry and the diversity of various membranes.

4.5 Structure of organelle membranes

Because of the long history of the hypothesis that all membranes in cells have a similar structure, organelle membranes were speculated to be the same as cell membranes. As previously discussed, we have clear results that demonstrate the structures of membranes differ according to their functions. Thus, what is the structure of organelle membranes? Two main organelle membranes (the Golgi apparatus and mitochondrial membranes) were imaged using situ AFM (Figure 22).[140-141] The mitochondrial and Golgi membranes exhibit features similar to red blood cell membranes, that is, the outer surface is flat with protruding proteins located in the inner side (Table 2). In addition, whether there is a lipid raft domain in endocytotic membranes was unclear before Wang et al. directly visualized a Golgi vesicle that was eroded using Triton-100 and MβCD.[140] The size of the lipid rafts in Golgi membranes is very similar to that in red blood cell membranes. The results from endomembrane structure studies confirm that the membrane protein distribution is asymmetrical, which is similar to the structure of red blood cell membranes.

In Table 2, we summarize the thickness of membranes (lipid bilayer + outer layer) without the inclusion of cytoplasmic protein particle measurements. The red blood cell and Golgi membrane exhibit very similar features. The nucleated mammalian cell membranes and mitochondrial membranes are substantially thicker than the red blood cell membranes. Notably, the thickness of a lipid bilayer is approximately 3.0 nm, which is close to the thickness of red blood cell and Golgi membranes and indicates that there is no outer protein layer for these membranes.

5. Examination of cell membranes via SMFS

5.1 Identification of the mechanism of interactions between membrane proteins and ligands using SMFS

Biological interactions in cells are based on force.[142-145] The interaction force for these molecules is on the scale of tens of piconewtons. To measure these weak

interactions, several techniques are available,[146] such as AFM,[147] optical tweezers and magnetic tweezers.[148] An AFM-based force curve can detect forces in a large range from 10 pN to 100 nN, which is wider than the range of other competing techniques.[146]

In a living cell, an environmental signal is transduced into the cell via a membrane receptor. The interaction force between a ligand and its receptor is the main feature that signals activation. Force curves have been used to study multiple interactions between cell membrane proteins and ligands, and these curves can provide insightful information regarding the energy landscape of membrane receptors and their ligands. The dynamic information of a force curve can be deduced from the equation of Evans et al.[149] Tang et al. studied the interactions between a hormone (luteinizing hormone-releasing hormone) and its receptor.[150] Hinterdorfer et al. explored the interactions between the serotonin transporter and a cocaine analog in living cells using SMFS,[151] mapped the interaction energy landscape, and derived chemical rate constants. The receptor interaction model can be determined using SMFS at the single-molecule level. Fang et al. detected the interactions of HER2 and epidermal grown factor receptors (EGFRs)[152] and demonstrated that cancer therapy antibodies (Trastuzumab and Pertuzumab) target HER2 to interrupt the interaction between HER2 and EGFR, which results in a decrease in the downstream signaling of EGFRs. The transport process is dynamic and accompanied by a conformational change in the transporter. Using dynamic SMFS, Muller et al. demonstrated that substrate binding can change the kinetics, energetics, and mechanical properties of the ectoplasmic 6-helix bundle of LacY, but not the cytoplasmic part, to facilitate substrate transportation.[153]

Viral attachment to the membrane prior to infection is mediated by a membrane receptor. Because a virus is larger than a single molecule and includes multiple ligands, more than one binding site is expected. Using AFM force spectroscopy, Herrmann et al. verified this hypothesis to demonstrate that multiple viral binding modes occurred during infection.[154-155]

5.2 Examination of the dynamic function of cell membranes using SMFS

The cell membrane has dynamic functions for material transport, including endocytosis and transport by membrane proteins. The SMFS detection speed is unprecedentedly high (up to 10 μs),[146] which is suitable for the measurement of fast processes in a living cell system. Researchers typically used the retrace peak curve in a force curve to measure the molecular interactions; during these measurements, the sample is statically immobilized on the surface. Interestingly, Wang et al. extended

the force curve to measure dynamic processes of cell membranes by recording both the tracing and retracing events. The tracing curve is used to record the uptake events of membranes. Similar to the fishing concept, nanoparticles (e.g., QDs and gold nanoparticles) are attached to the AFM tip (Figure 23), and the endocytosis force of nanoparticles is detected.[156-157] The coupled force events (uptake by cell membranes and withdrawal of the AFM tip) are features of the dynamic process of cell membranes. The force of transporting a single molecule (e.g., amino acid) into a living cell was further measured using SMFS.[158] The maximum distribution of the transporting force "fi" is approximately 66 pN, and the maximum distribution of the unbinding force "fu" is approximately 70 pN. Importantly, the measurement indicates that the conformation of the transporter determines the transporting events. These results provide new insights into the dynamic mechanism of material transport via cell membranes at the single-molecule (or particle) level.

One technical restriction must be considered when recording transport events. Low force should be engaged during force measurement (less than 1 nN, typically 500 pN) to prevent membrane breakage. For AFM tip penetration, the force must be at least 2 nN to break the cell membrane;[159] this force differs from the force required to measure the transport events. In addition, a blunt AFM tip will be ideal to avoid the tip penetration issue.

6. Significance and outlook

With the development of nanotechnology, advances in imaging techniques have deepened our understanding of the cell membrane, which represents a supramolecular structure. AFM directly visualizes the whole cell membrane in situ; in particular, in situ enzyme digestion with in situ AFM can locate entire proteins in membranes. The "top-down" dissection and observation by AFM provides an unprecedented opportunity to determine the sophisticated structure of membranes. A new structure and characteristics of cell membranes have been identified via AFM (Table 3).

In situ AFM provides a complete picture of various membranes, including red blood cell membranes, nucleated cell membranes and endomembranes. These studies describe two main features: membrane structures vary according to the membrane type, and the asymmetry of cell membranes is universal.

The membrane structure is so complicated that one model cannot describe all aspects of membranes. The debate regarding membranes may soon be terminated because membranes could assume multiple features, such as a lipid bilayer, protein mosaicism, liquidity, cholesterol-enriched raft domains, non-raft domains and a dense

protein layer. The complete picture identified via AFM will shed light on the most sophisticated structure, i.e., the structure of cell membranes.

These novel models provide appropriate explanations for the key characteristics of cell membranes: 1. The membrane of eukaryotic cells is inextensible and easily ruptured under in-plane tension, such as osmotic stress;[160] however, the membrane exhibits an endocytic activity by membrane invagination in living cells. The explanation is that the dense protein layer on the outer surface and isolated protein domains in the inner side generate membrane tension in one direction. 2. Why can a hypotonic solution easily burst red blood cells but not nucleated mammalian cells? The explanation is that the RBC membrane is thin, and there is no outer dense protein layer to protect the lipid bilayer. 3. The mechanical characteristics (ductility) of nucleated cell membranes suggest that these membranes are much better suited than the model membrane (SLBs) to defend against environmental attack. The explanation is that the dense protein layer in membranes is the main contributor to membrane stability. 4. Why is there only vesicle endocytosis but not the ejection of membrane vesicles from the cell membrane? The explanation is that the outer membrane layer experiences tension from the outer surface, which makes it unable to eject vesicles off the membranes, although there are motor proteins in the cytoplasm. 5. Why is the membrane transportation directed from the cell membrane to an endocytic vesicle, while the endomembrane shape remains constant (e.g., the Golgi apparatus, a typical cytoplasmic membrane vesicle that is pivotal for cellular transport, exhibits a directional transportation from the Golgi to the membrane or from the membrane to the Golgi without membrane fusion that alters the composition of the target)? The explanation is that the asymmetry of endocytic vesicles from cell membranes is opposite to the endomembrane vesicle; endocytic vesicles can only function as a shuttle for membrane recycling but cannot become a part of an endomembrane by membrane fusion. The interactions of these vesicles may follow the kiss-and-run principle but not membrane fusion, which enables efficient membrane transport and vesicle stability. 6. What is the relationship between the proteins in lipid rafts and the non-lipid raft proteins? Based on the structure of a nucleated cell membrane, some proteins exist in lipid rafts. However, lipid rafts are only local domains in a dense protein layer; they are not isolated carriers in lipid bilayers. The dense protein layer consists of both lipid rafts and non-lipid raft proteins.

In addition to the experimental efforts to study the cell membrane, molecular simulation is an important approach to identifying the dynamic features of cell membranes.[161] However, to date, molecular dynamic (MD) simulation is only suitable for a model membrane (proteins in a lipid bilayer). How the proteins in a complicated

cell membrane work remains an unresolved question. A novel membrane structure may provide useful information for accurate predictions from MD simulation because the membrane protein environment could be a significant factor in obtaining accurate simulations.

There are still open questions regarding membrane structure; for example, the accurate location of membrane proteins in the membrane, the membrane protein relationships, and the mechanism that underlies the formation of the protein pattern. These questions may be solved via the combination of multiple techniques, such as in situ AFM, super-resolution fluorescence microscopy, cryo-EM, MS, and enzymatic methods.[62] The combination of AFM with fluorescence microscopy will provide additional information regarding the cell membrane structure and characteristics.[116, 162-163] Super-resolution fluorescence microscopy provides the potent ability to identify the local architecture of cell membranes.[164-165] Cryo-EM may contribute knowledge regarding the protein arrangement of cell membranes at a subnanometer resolution[166]. The results obtained using all of these techniques suggest that a comprehensive membrane structure could be expected in the near future with the further development of single-molecule techniques.

Acknowledgements

This work was supported by MOST (grant no. 2011CB933600 to H.W.), NSFC (Grant no. 21373200 to H.W; Grant no. 31330082 and 21303181 to Y.S.).

References

1. B. Alberts, A. Johnson, J. Lewis, M. Raff, K. Roberts and P. Walter, *Molecular Biology of the Cell*, Garland Science, 5th edition, New York, 2008.
2. G. Raposo and W. Stoorvogel, *J. Cell Biol.*, 2013, 200, 373-383.
3. K. Simons and D. Toomre, *Nat. Rev. Mol. Cell Biol.*, 2000, 1, 31-39.
4. B. Glancy and R. S. Balaban, *Biochemistry*, 2012, 51, 2959-2973.
5. J. C. Sacchettini, L. G. Baum and C. F. Brewer, *Biochemistry*, 2001, 40, 3009-3015.
6. P. Vandenabeele, L. Galluzzi, T. Vanden Berghe and G. Kroemer, *Nat. Rev. Mol. Cell Biol.*, 2010, 11, 700-714.
7. J. W. Szostak, D. P. Bartel and P. L. Luisi, *Nature*, 2001, 409, 387-390.
8. Q. S. Li, G. Y. H. Lee, C. N. Ong and C. T. Lim, *Biochem. Biophys. Res. Commun.*, 2008, 374, 609-613.
9. Y. F. Dufrene, *Nat. Protoc.*, 2008, 3, 1132-1138.

10. P. E. Milhiet, P. Dosset, C. Godefroy, C. Le Grimellec, J. M. Guigner, E. Larquet, F. Ronzon and C. Manin, *Biochimie*, 2011, 93, 254-259.
11. G. Karp, *Cell and molecular biology: concepts and experiments,* John Wiley & Sons, 4th edition, New Jersey, 2005, pp. 121-181.
12. A. Varki, *Glycobiology*, 1993, 3, 97-130.
13. T. J. Stevens and I. T. Arkin, *PROTEINS*, 2000, 39, 417-420.
14. M. S. Almen, K. J. V. Nordstrom, R. Fredriksson and H. B. Schioth, *BMC Biol.*, 2009, 7:50, doi:10.1186/1741-7007-7-50.
15. J. Schiller, R. Suss, B. Fuchs, M. Muller, O. Zschornig and K. Arnold, *Front. Biosci.*, 2007, 12, 2568-2579.
16. E. Gorter and F. Grendel, *J. Exp. Med.*, 1925, 41, 439-443.
17. K. S. Cole, *J. Cell. Comp. Physiol.*, 1932, 1, 1-9.
18. J. F. Danielli and E. N. Harvey, *J. Cell. Comp. Physiol.*, 1935, 5, 483-494.
19. J. F. Danielli and H. Davson, *J. Cell. Comp. Physiol.*, 1935, 5, 495-508.
20. F. S. Sjostrand, E. Anderssoncedergren and M. M. Dewey, *J. Ultrastruct. Res.*, 1958, 1, 271-287.
21. J. D. Robertson, *Biochem. Soc. Symposium*, 1959, 16, 3-43.
22. S. J. Singer and G. L. Nicolson, *Science*, 1972, 175, 720-731.
23. D. M. Engelman, *Nature*, 2005, 438, 578-580.
24. D. A. Brown and J. K. Rose, *Cell*, 1992, 68, 533-544.
25. D. Lingwood and K. Simons, *Science*, 2010, 327, 46-50.
26. K. Simons and E. Ikonen, *Nature*, 1997, 387, 569-572.
27. C. Eggeling, C. Ringemann, R. Medda, G. Schwarzmann, K. Sandhoff, S. Polyakova, V. N. Belov, B. Hein, C. von Middendorff, A. Schoenle and S. W. Hell, *Nature*, 2009, 457, 1159-1162.
28. Y. Wang, J. Gao, X. Guo, T. Tong, X. Shi, L. Li, M. Qi, Y. Wang, M. Cai, J. Jiang, C. Xu, H. Ji and H. Wang, *Cell Res.*, 2014, 24, 959-976.
29. A. M. Whited and P. S. H. Park, *Biochim. Biophys. Acta-Biomembr.*, 2014, 1838, 56-68.
30. M. Zocher, C. A. Bippes, C. Zhang and D. J. Muller, *Chem. Soc. Rev.*, 2013, 42, 7801-7815.
31. S. Zhang, H. Aslan, F. Besenbacher and M. Dong, *Chem. Soc. Rev.*, 2014, 43, 7412-7429.
32. T. Xia, N. Li and X. Fang, *Annu. Rev. Phys. Chem.,* Vol. 64, 2013, 64, 459-480.
33. A. Engel and H. E. Gaub, *Annu. Rev. Biochem.*, 2008, 77, 127-148.
34. D. J. Taatjes, A. S. Quinn, J. H. Rand and B. P. Jena, *J. Cell. Physiol.*, 2013, 228, 1949-1955.

35. H. P. Lu, *Chem. Soc. Rev.*, 2014, 43, 1118-1143.
36. Y. G. Kuznetsov, T. Klose, M. Rossmann and A. McPherson, *J. Virol.*, 2013, 87, 11200-11213.
37. M. Gladnikoff and I. Rousso, *Biophys. J.*, 2008, 94, 320-326.
38. M. T. Woodside and S. M. Block, *Annu. Rev. Biophys.*, 2014, 43, 19-39.
39. P. Hinterdorfer and Y. F. Dufrene, *Nat. Methods*, 2006, 3, 347-355.
40. Y. F. Dufrene, D. Martinez-Martin, I. Medalsy, D. Alsteens and D. J. Mueller, *Nat. Methods*, 2013, 10, 847-854.
41. G. Binnig, C. F. Quate and C. Gerber, *Phys. Rev. Lett.*, 1986, 56, 930-933.
42. D. Fotiadis, *Curr. Opin. Biotechnol.*, 2012, 23, 510-515.
43. Y. J. Song, A. F. Otte, V. Shvarts, Z. Y. Zhao, Y. Kuk, S. R. Blankenship, A. Band, F. M. Hess and J. A. Stroscio, *Rev. Sci. Instrum.*, 2010, 81.
44. D. J. Muller, G. M. Hand, A. Engel and G. E. Sosinsky, *EMBO J.*, 2002, 21, 3598-3607.
45. R. Garcia and R. Perez, *Surf. Sci. Rep.*, 2002, 47, 197-301.
46. Y. Gan, *Surf. Sci. Rep.*, 2009, 64, 99-121.
47. P. K. Hansma, J. P. Cleveland, M. Radmacher, D. A. Walters, P. E. Hillner, M. Bezanilla, M. Fritz, D. Vie, H. G. Hansma, C. B. Prater, J. Massie, L. Fukunaga, J. Gurley and V. Elings, *Appl. Phys. Lett.*, 1994, 64, 1738-1740.
48. D. A. Walters, M. Viani, G. T. Paloczi, T. E. Schaeffer, J. P. Cleveland, M. A. Wendman, G. Gurley, V. B. Elings and P. K. Hansma, *Proceedings of the society of photo-optical instrumentation engineers (SPIE)*, 1997, 3009, 43-47.
49. M. B. Viani, L. I. Pietrasanta, J. B. Thompson, A. Chand, I. C. Gebeshuber, J. H. Kindt, M. Richter, H. G. Hansma and P. K. Hansma, *Nat. Struct. Mol. Biol.*, 2000, 7, 644-647.
50. F. Kienberger, C. Stroh, G. Kada, R. Moser, W. Baumgartner, V. Pastushenko, C. Rankl, U. Schmidt, H. Muller, E. Orlova, C. LeGrimellec, D. Drenckhahn, D. Blaas and P. Hinterdorfer, *Ultramicroscopy*, 2003, 97, 229-237.
51. N. Jalili and K. Laxminarayana, *Mechatronics*, 2004, 14, 907-945.
52. L. A. Chtcheglova and P. Hinterdorfer, *J. Mol. Recognit.*, 2011, 24, 788-794.
53. C. Stroh, H. Wang, R. Bash, B. Ashcroft, J. Nelson, H. Gruber, D. Lohr, S. M. Lindsay and P. Hinterdorfer, *P. Natl. Acad. Sci. USA.*, 2004, 101, 12503-12507.
54. S. Lee, J. Mandic and K. J. Van Vliet, *P. Natl. Acad. Sci. USA.*, 2007, 104, 9609-9614.
55. M. Pfreundschuh, D. Alsteens, M. Hilbert, M. O. Steinmetz and D. J. Müller, *Nano Lett.*, 2014, 14, 2957-2964.
56. T. Uchihashi, R. Iino, T. Ando and H. Noji, *Science*, 2011, 333, 755-758.

57. T. Ando, T. Uchihashi and T. Fukuma, *Prog. Surf. Sci.*, 2008, 83, 337-437.
58. Y. Shinozaki, K. Sumitomo, M. Tsuda, S. Koizumi, K. Inoue and K. Torimitsu, *PLoS. Biol.*, 2009, 7, e1000103. doi:10.1371/journal.pbio.1000103.
59. T. Ando, *FEBS Lett.*, 2013, 587, 997-1007.
60. N. Kodera, D. Yamamoto, R. Ishikawa and T. Ando, *Nature*, 2010, 468, 72-76.
61. Y. Suzuki, N. Sakai, A. Yoshida, Y. Uekusa, A. Yagi, Y. Imaoka, S. Ito, K. Karaki and K. Takeyasu, *Sci. Rep.*, 2013, 3, 2131.
62. A. Colom, I. Casuso, F. Rico and S. Scheuring, *Nat. Commun.*, 2013, 4.
63. T. Ando, *Nanotechnology*, 2012, 23, 062001.
64. H. D. Wang, R. Bash, J. G. Yodh, G. L. Hager, D. Lohr and S. M. Lindsay, *Biophys. J.*, 2002, 83, 3619-3625.
65. D. Lohr, R. Bash, H. Wang, J. Yodh and S. Lindsay, *Methods*, 2007, 41, 333-341.
66. A. Noy, *Curr. Opin. Chem. Biol.*, 2011, 15, 710-718.
67. T. Hoffmann and L. Dougan, *Chem. Soc. Rev.*, 2012, 41, 4781-4796.
68. J. Alegre-Cebollada, P. Kosuri, D. Giganti, E. Eckels, J. A. Rivas-Pardo, N. Hamdani, C. M. Warren, R. J. Solaro, W. A. Linke and J. M. Fernandez, *Cell*, 2014, 156, 1235-1246.
69. I. Popa, P. Kosuri, J. Alegre-Cebollada, S. Garcia-Manyes and J. M. Fernandez, *Nat. Protoc.*, 2013, 8, 1261-1276.
70. E. L. Florin, V. T. Moy and H. E. Gaub, *Science*, 1994, 264, 415-417.
71. F. Schwesinger, R. Ros, T. Strunz, D. Anselmetti, H.-J. Guntherodt, A. Honegger, L. Jermutus, L. Tiefenauer and A. Pluckthun, *Proc. Natl. Acad. Sci. US.A*, 2000, 97, 9972-9977.
72. M. Rief, H. Clausen-Schaumann and H. E. Gaub, *Nat. Struct. Mol. Biol.*, 1999, 6, 346-349.
73. G. Lee, L. Chrisey and R. Colton, *Science*, 1994, 266, 771-773.
74. M. Rief, M. Gautel, F. Oesterhelt, J. M. Fernandez and H. E. Gaub, *Science*, 1997, 276, 1109-1112.
75. M. Rief, F. Oesterhelt, B. Heymann and H. E. Gaub, *Science*, 1997, 275, 1295-1297.
76. J. M. Fernandez and H. B. Li, *Science*, 2004, 303, 1674-1678.
77. A. P. Wiita, R. Perez-Jimenez, K. A. Walther, F. Graeter, B. J. Berne, A. Holmgren, J. M. Sanchez-Ruiz and J. M. Fernandez, *Nature*, 2007, 450, 124-127.
78. P. Hinterdorfer, W. Baumgartner, H. J. Gruber, K. Schilcher and H. Schindler, *Natl. Acad. Sci. USA.*, 1996, 93, 3477-3481.

79. Y. Shen, J. L. Sun, A. Zhang, J. Hu and L. X. Xu, *Phys. Med. Biol.* , 2007, 52, 2185-2196.
80. H. J. Butt, B. Cappella and M. Kappl, *Surf. Sci. Rep.*, 2005, 59, 1-152.
81. Y. F. Dufrene and M. F. Garcia-Parajo, *Nano Today*, 2012, 7, 390-403.
82. H. D. Wang, L. Obenauer-Kutner, M. Lin, Y. P. Huang, M. J. Grace and S. M. Lindsay, *J. Am. Chem. Soc.*, 2008, 130, 8154-8155.
83. D. J. Muller, D. Fotiadis, S. Scheuring, S. A. Muller and A. Engel, *Biophys. J.*, 1999, 76, 1101-1111.
84. S. Scheuring, D. Levy and J. L. Rigaud, *Biochim. Biophys. Acta-Biomembr.*, 2005, 1712, 109-127.
85. D. J. Muller and A. Engel, *Nat. Protoc.*, 2007, 2, 2191-2197.
86. R. Garcia and E. T. Herruzo, *Nat. Nanotechnol.*, 2012, 7, 217-226.
87. J. Wu, J. Gao, M. Qi, J. Wang, M. Cai, S. Liu, X. Hao, J. Jiang and H. Wang, *Nanoscale*, 2013, 5, 11582-11586.
88. R. P. Goncalves, G. Agnus, P. Sens, C. Houssin, B. Bartenlian and S. Scheuring, *Nat. Methods*, 2006, 3, 1007-1012.
89. K. H. Tantawi, B. Berdiev, R. Cerro and J. D. Williams, *Superlattice. Microst.*, 2013, 58, 72-80.
90. A. Pietuch, B. R. Bruckner, T. Fine, I. Mey and A. Janshoff, *Soft Matter*, 2013, 9, 11490-11502.
91. H. Schillers, *Pflugers Arch.*, 2008, 456, 163-177.
92. H. D. Wang, X. Hao, Y. P. Shan, J. G. Jiang, M. J. Cai and X. Shang, *Ultramicroscopy*, 2010, 110, 305-312.
93. M. Takeuchi, H. Miyamoto, Y. Sako, H. Komizu and A. Kusumi, *Biophys. J.*, 1998, 74, 2171-2183.
94. W. Zhao, Y. Tian, M. Cai, F. Wang, J. Wu, J. Gao, S. Liu, J. Jiang, S. Jiang and H. Wang, *PLoS One*, 2014, 9:e91595. doi:10.1371/journal.pone.0091595.
95. J. Usukura, A. Yoshimura, S. Minakata, D. Youn, J. Ahn and S. J. Cho, *J. Electron Microsc.*, 2012, 61, 321-326.
96. D. J. Frankel, J. R. Pfeiffer, Z. Surviladze, A. E. Johnson, J. M. Oliver, B. S. Wilson and A. R. Burns, *Biophys. J.*, 2006, 90, 2404-2413.
97. C. Marasini, E. Jacchetti, M. Moretti, C. Canale, O. Moran and M. Vassalli, *Microsc. Res. Tech.*, 2013, 76, 723-732.
98. J. M. Lau, H. X. You and L. Yu, *Scanning*, 2002, 24, 224-231.
99. F. Orsini, M. Santacroce, P. Arosio, M. Castagna, C. Lenardi, G. Poletti and F. V. Sacchi, *Eur. Biophys. J. Biophys. Lett.*, 2009, 38, 903-910.

100. M. A. Hayat, *Micron Microsc. Acta*, 1986, 17, 115-135.
101. S. Morandat, S. Azouzi, E. Beauvais, A. Mastouri and K. El Kirat, *Anal. Bioanal. Chem.*, 2013, 405, 1445-1461.
102. K. Bacia, D. Scherfeld, N. Kahya and P. Schwille, *Biophys. J.*, 2004, 87, 1034-1043.
103. N. Kahya, D. Scherfeld, K. Bacia, B. Poolman and P. Schwille, *J. Biol. Chem.*, 2003, 278, 28109-28115.
104. H. M. McConnell, L. K. Tamm and R. M. Weis, *P. Natl. Acad. Sci. USA.*, 1984, 81, 3249-3253.
105. H. A. Rinia, R. A. Demel, J. van der Eerden and B. de Kruijff, *Biophys. J.*, 1999, 77, 1683-1693.
106. L. Picas, P.-E. Milhiet and J. Hernandez-Borrell, *Chem. Phys. Lipids*, 2012, 165, 845-860.
107. K. Simons and W. L. C. Vaz, *Annu. Rev. Biophys. Biomolec. Struct.*, 2004, 33, 269-295.
108. S. Morandat and K. El Kirat, *Langmuir*, 2006, 22, 5786-5791.
109. K. El Kirat and S. Morandat, *Biochim. Biophys. Acta-Biomembr.*, 2007, 1768, 2300-2309.
110. C. B. Yuan, J. Furlong, P. Burgos and L. J. Johnston, *Biophys. J.*, 2002, 82, 2526-2535.
111. A. Sumino, T. Sumikama, M. Iwamoto, T. Dewa and S. Oiki, *Sci. Rep.*, 2013, 3.
112. K. Simons and M. J. Gerl, *Nat. Rev. Mol. Cell Biol.*, 2010, 11, 688-699.
113. L. Rajendran and K. Simons, *J. Cell Sci.*, 2005, 118, 1099-1102.
114. J. S. Rossman and R. A. Lamb, *Virology*, 2011, 411, 229-236.
115. C. Neumann-Giesen, B. Falkenbach, P. Beicht, S. Claasen, G. Luers, C. A. O. Stuermer, V. Herzog and R. Tikkanen, *Biochem. J.*, 2004, 378, 509-518.
116. J. E. Shaw, R. F. Epand, R. M. Epand, Z. G. Li, R. Bittman and C. M. Yip, *Biophys. J.*, 2006, 90, 2170-2178.
117. A. S. Shaw, *Nat. Immunol.*, 2006, 7, 1139-1142.
118. F. Orsini, A. Cremona, P. Arosio, P. A. Corsetto, G. Montorfano, A. Lascialfari and A. M. Rizzo, *Biochim. Biophys. Acta-Biomembr.*, 2012, 1818, 2943-2949.
119. M. J. Cai, W. D. Zhao, X. Shang, J. G. Jiang, H. B. Ji, Z. Y. Tang and H. D. Wang, *Small*, 2012, 8, 1243-1250.
120. J. L. Cacas, F. Furt, M. Le Guedard, J. M. Schmitter, C. Bure, P. Gerbeau-Pissot, P. Moreau, J. J. Bessoule, F. Simon-Plas and S. Mongrand, *Prog. Lipid Res.*, 2012, 51, 272-299.
121. L. Wu, J. Huang, X. Yu, X. Zhou, C. Gan, M. Li and Y. Chen, *J. Membr. Biol.*,

2014, 247, 189-200.
122. G. R. Chichili and W. Rodgers, *J. Biol. Chem.*, 2007, 282, 36682-36691.
123. M. Sun, N. Northup, F. Marga, T. Huber, F. J. Byfield, I. Levitan and G. Forgacs, *J. Cell Sci.*, 2007, 120, 2223-2231.
124. M. Murakoshi, T. Gomi, K. Iida, S. Kumano, K. Tsumoto, I. Kumagai, K. Ikeda, T. Kobayashi and H. Wada, *JARO*, 2006, 7, 267-278.
125. F. M. Ohnesorge, J. K. H. Horber, W. Haberle, C.-P. Czerny, D. P. E. Smith and a. G. Binnig, *Biophys. J.*, 1997, 73, 2183-2194.
126. S. Eisenberg, D. E. Shvartsman, M. Ehrlich and Y. I. Henis, *Mo. Cell. Biol.*, 2006, 26, 7190-7200.
127. P. Sengupta, B. Baird and D. Holowka, *Semin. Cell Dev. Biol.*, 2007, 18, 583-590.
128. T. Gonen, Y. F. Cheng, P. Sliz, Y. Hiroaki, Y. Fujiyoshi, S. C. Harrison and T. Walz, *Nature*, 2005, 438, 633-638.
129. Y. P. Shan, Z. Y. Wang, X. A. Hao, X. Shang, M. J. Cai, J. G. Jiang, X. X. Fang, H. D. Wang and Z. Y. Tang, *Anal. Methods*, 2010, 2, 805-808.
130. J. G. Jiang, X. Hao, M. J. Cai, Y. P. Shan, X. Shang, Z. Y. Tang and H. D. Wang, *Nano Lett.*, 2009, 9, 4489-4493.
131. A. Ebner, D. Nikova, T. Lange, J. Haberle, S. Falk, A. Dubbers, R. Bruns, P. Hinterdorfer, H. Oberleithner and H. Schillers, *Nanotechnology*, 2008, 19.
132. J. Kiernan, *Microscopy Today*, 00-1 pp. 8-12 (2000).
133. Y. Tian, M. Cai, W. Zhao, S. Wang, Q. Qin and H. Wang, *Chinese Sci. Bull.*, 2014, 59, 2582-2587.
134. Y. Tian, M. Cai, H. Xu, B. Ding, X. Hao, J. Jiang, Y. Sun and H. Wang, *Mol. Cells*, 2014, 37, 592-597.
135. Y. Tian, M. Cai, H. Xua and H. Wang, *Anal. Methods*, 2014, 6, 8115-8119.
136. M. Murakoshi, K. Iida, S. Kumano and H. Wada, *Pflugers Arch.*, 2009, 457, 885-898.
137. L. Dindia, E. Faught, Z. Leonenko, R. Thomas and M. M. Vijayan, *Am. J. Physiol-Endoc. M.*, 2013, 304, E1157-E1166.
138. J. Zhang, L. A. Chtcheglova, R. Zhu, P. Hinterdorfer, B. L. Zhang and J. L. Tang, *Anal. Chem.*, 2014, 86, 2458-2464.
139. G. L. Nicolson, *Biochim. Biophys. Acta-Biomembr.*, 2014, 1838, 1451-1466.
140. H. J. Xu, W. H. Su, M. J. Cai, J. G. Jiang, X. L. Zeng and H. D. Wang, *PLoS One*, 2013, 8: e61596. doi:10.1371/journal.pone.0061596.
141. Y. Tian, J. Li, M. Cai, W. Zhao, H. Xu, Y. Liu and H. Wang, *RSC Adv.*, 2013, 3, 708-712.

142. C. M. Franz and P. H. Puech, *Cell. Mol. Bioeng.*, 2008, 1, 289-300.
143. I. Casuso, F. Rico and S. Scheuring, *J. Mol. Recognit.*, 2011, 24, 406-413.
144. Y. Gilbert, M. Deghorain, L. Wang, B. Xu, P. D. Pollheimer, H. J. Gruber, J. Errington, B. Hallet, X. Haulot, C. Verbelen, P. Hols and Y. F. Dufrêne, *Nano Lett.*, 2007, 7, 796-801.
145. K. X. Hu, F. H. Zhao and Q. K. Wang, *Proceedings of the Institution of Mechanical Engineers Part H-Journal of Engineering in Medicine*, 2013, 227, 1319-1323.
146. H. Clausen-Schaumann, M. Seitz, R. Krautbauer and H. E. Gaub, *Curr. Opin. Chem. Biol.*, 2000, 4, 524-530.
147. E. M. Puchner and H. E. Gaub, *Curr. Opin. Struct. Biol.*, 2009, 19, 605-614.
148. K. C. Neuman and A. Nagy, *Nat. Methods*, 2008, 5, 491-505.
149. E. Evans and K. Ritchie, *Biophys. J.*, 1997, 72, 1541-1555.
150. J. Zhang, G. M. Wu, C. L. Song, Y. J. Li, H. Y. Qiao, P. Zhu, P. Hinterdorfer, B. L. Zhang and J. L. Tang, *J. Phys. Chem. B*, 2012, 116, 13331-13337.
151. L. Wildling, C. Rankl, T. Haselgrubler, H. J. Gruber, M. Holy, A. H. Newman, M. F. Zou, R. Zhu, M. Freissmuth, H. H. Sitte and P. Hinterdorfer, *J. Biol. Chem.*, 2012, 287, 105-113.
152. X. J. Zhang, X. L. Shi, L. Xu, J. H. Yuan and X. H. Fang, *Nanomed. Nanotechnol.*, 2013, 9, 627-635.
153. T. Serdiuk, M. G. Madej, J. Sugihara, S. Kawamura, S. A. Mari, H. R. Kaback and D. J. Mueller, *P. Natl. Acad. Sci. USA.*, 2014, 111, E1571-E1580.
154. C. Sieben, C. Kappel, R. Zhu, A. Wozniak, C. Rankl, P. Hinterdorfer, H. Grubmueller and A. Herrmann, *P. Natl. Acad. Sci. USA.*, 2012, 109, 13626-13631.
155. C. Rankl, F. Kienberger, L. Wildling, J. Wruss, H. J. Gruber, D. Blaas and P. Hinterdorfer, *P. Natl. Acad. Sci. USA.*, 2008, 105, 17778-17783.
156. Y. P. Shan, X. A. Hao, X. Shang, M. J. Cai, J. G. Jiang, Z. Y. Tang and H. D. Wang, *Chem. Commun.*, 2011, 47, 3377-3379.
157. Y. P. Shan, S. Y. Ma, L. Y. Nie, X. Shang, X. Hao, Z. Y. Tang and H. D. Wang, *Chem. Commun.*, 2011, 47, 8091-8093.
158. X. Shang, Y. Shan, Y. Pan, M. Cai, J. Jiang and H. Wang, *Chem. Commun.*, 2013, 49, 8163-8165.
159. A. Meister, M. Gabi, P. Behr, P. Studer, J. Voros, P. Niedermann, J. Bitterli, J. Polesel-Maris, M. Liley, H. Heinzelmann and T. Zambelli, *Nano Lett.*, 2009, 9, 2501-2507.
160. A. Pietuch, B. R. Bruckner and A. Janshoff, *BBA-Mol. Cell Res.*, 2013, 1833,

712-722.

161. H. Jang, L. Connelly, F. T. Arce, S. Ramachandran, B. L. Kagan, R. Lal and R. Nussinov, *J. Chem. Theory Comput.*, 2013, 9, 822-833.
162. S. H. Doak, D. Rogers, B. Jones, L. Francis, R. S. Conlan and C. Wright, *Histochem. Cell Biol.*, 2008, 130, 909-916.
163. J. Madl, S. Rhode, H. Stangl, H. Stockinger, P. Hinterdorfer, G. J. Schutz and G. Kada, *Ultramicroscopy*, 2006, 106, 645-651.
164. B. A. Truong-Quang and P. F. Lenne, *Front. Plant Sci.*, 2014, 5:18.doi:10.3389/fpls.2014.00018.
165. M. J. Rust, M. Bates and X. Zhuang, *Nat. Methods*, 2006, 3, 793-795.
166. X. Zhang, L. Jin, Q. Fang, W. H. Hui and Z. H. Zhou, *Cell*, 2010, 141, 472-482.

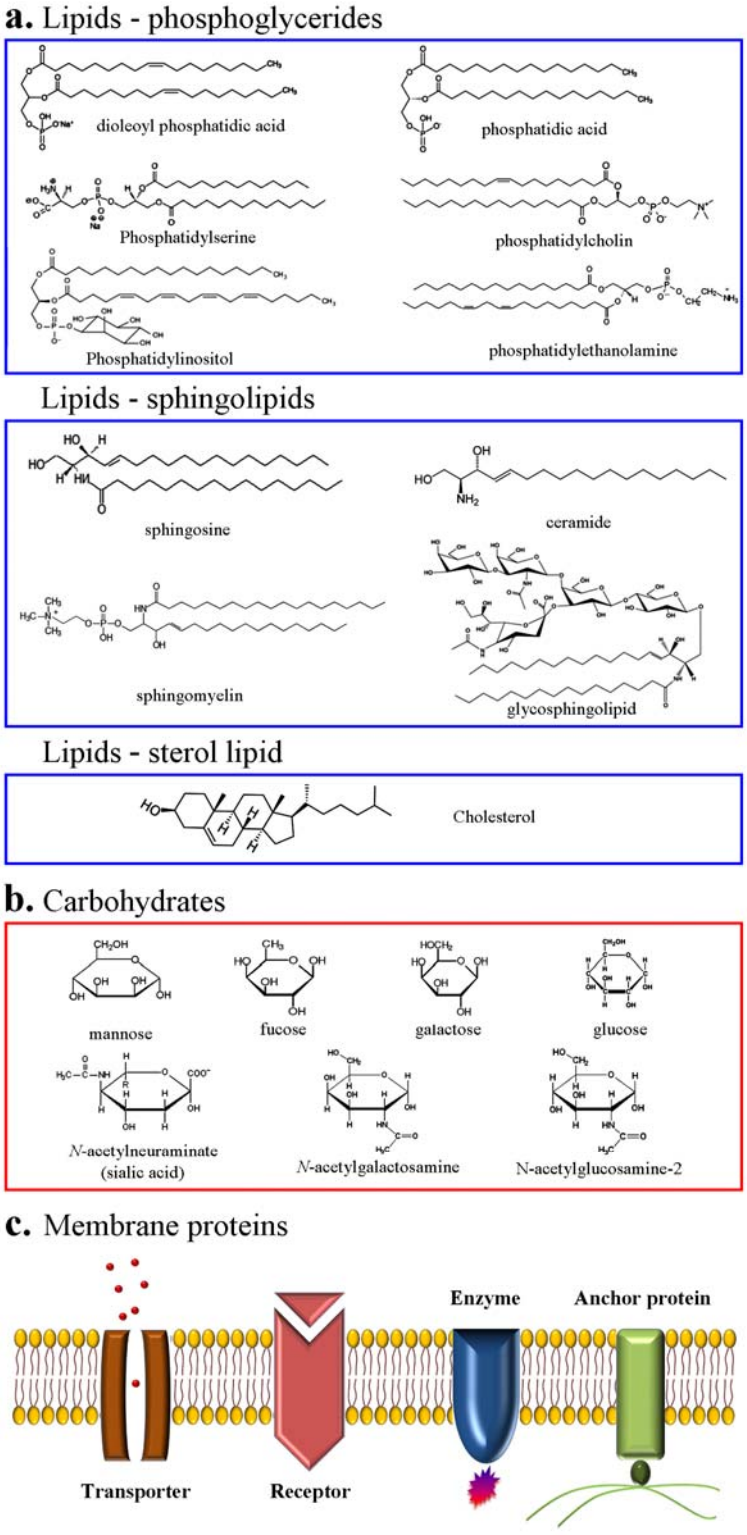

Figure 1. The basic components of cell membranes. (a) Membrane lipids mainly include phosphoglycerides, sphingolipids and sterol lipids. (b) Membrane carbohydrates include mannose, galactose, N-acetylglucosamine, glucose, fucose, N-acetylgalactosamine, sialic acid, and so on. (c) Membrane proteins refer to transporters, receptors, enzymes and anchor proteins.

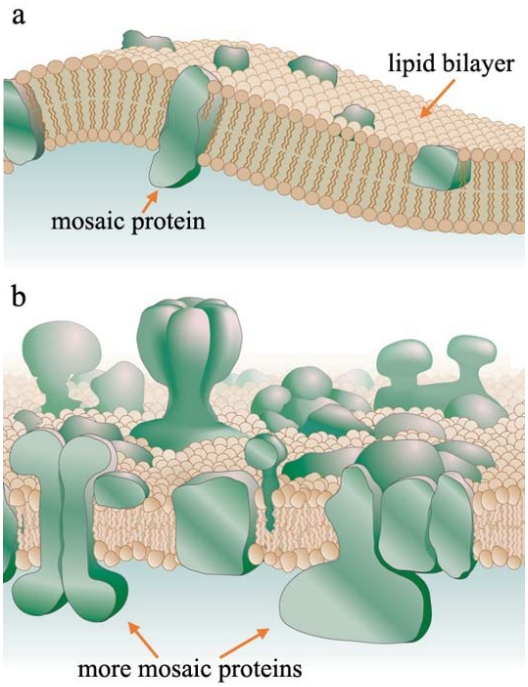

Figure 2. Models of membrane structure. (a) The Singer-Nicholson "fluid mosaic model". (b) An amended and updated version of the fluid mosaic model. Adapted from ref. 23 with permission copyright© 2005 Nature.

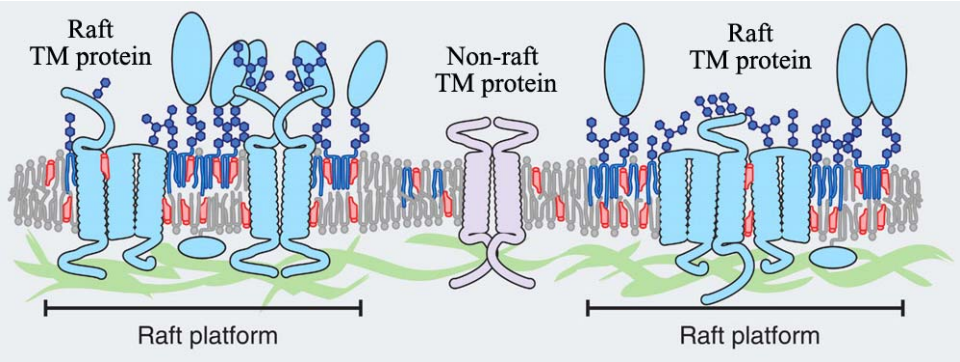

Figure 3. Lipid raft domains in cell membranes. Adapted from ref. 25 with permission copyright© 2010 Science.

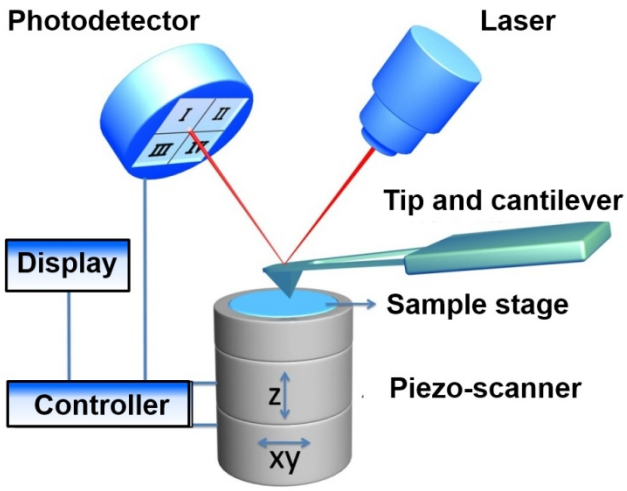

Figure 4. Schematic diagram of atomic force microscopy.

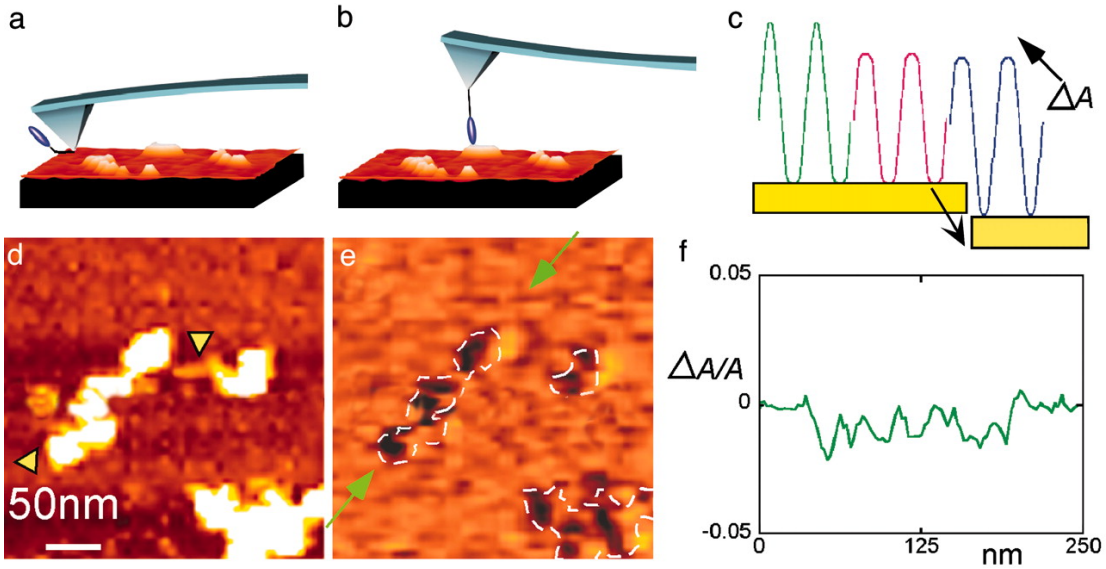

Figure 5. The principle of topography and recognition imaging. An AFM tip tethered to an antibody scans the sample (a, b). Antigen-antibody binding causes a transient reduction in the oscillation amplitude of the tip (c). The AFM feedback system converts this change to a recognition signal. (d, e) A topographic image of MMTV chromatin arrays and the corresponding recognition image. (f) A plot of the peak signal, ΔA, for the portion of the recognition image between the green arrows in (e). Adapted from ref. 53, Figure 1 with permission.

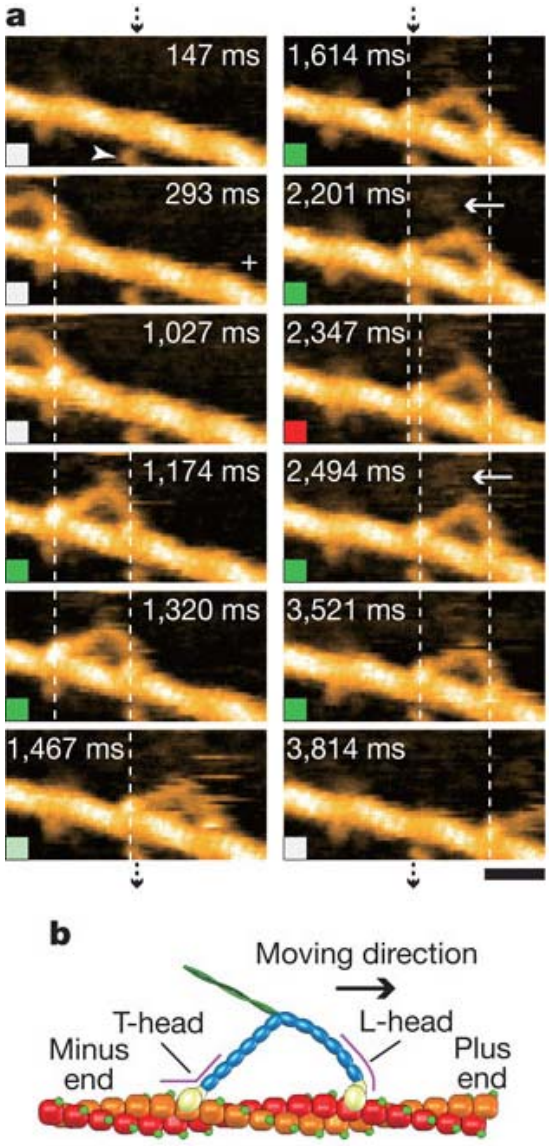

Figure 6. Imaging single molecules by high-speed AFM. (a) Successive AFM images that demonstrate the processive movement of M5-HMM in 1 μM ATP. Scale bar is 30 nm. (b) Schematic of two-headed bound M5-HMM. Adapted from ref. 60, Figures 1a and 1b with permission.

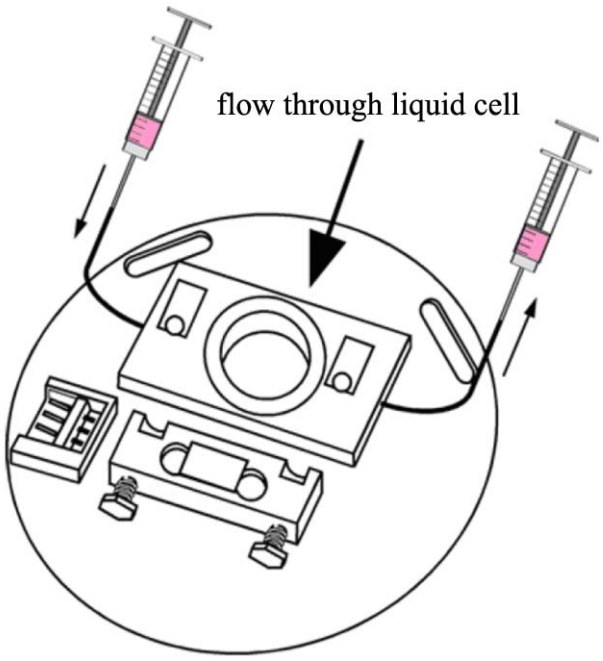

Figures 7. Schematic of fluid through a liquid cell. Adapted from ref. 65, Figure 3 with permission.

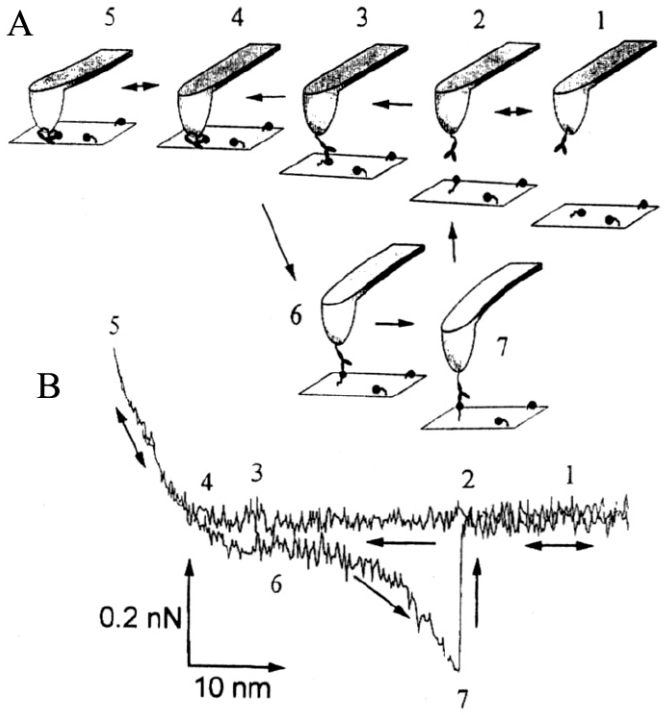

Figure 8. The process of single-molecule force spectroscopy. (a) An AFM tip tethered to an antibody engages the sample, which results in a force curve. The numbers 1-5 indicate the approach process. The numbers 6-7 indicate the withdrawal process. (b) A typical force-distance cycle corresponding to (a). Adapted from ref. 78, Figure 1 with permission.

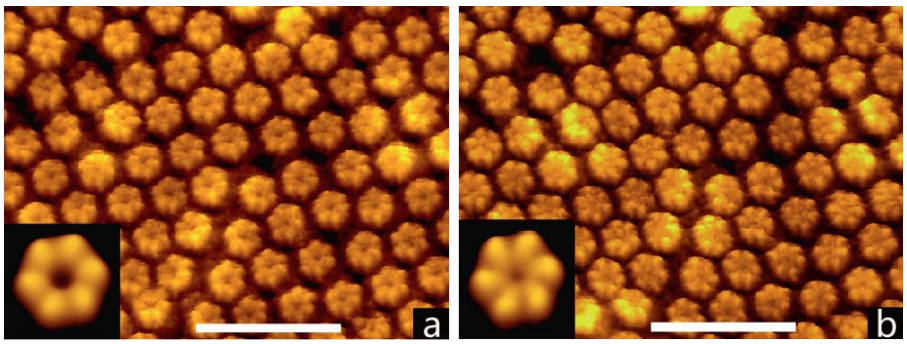

Figure 9. High-resolution AFM image of proteins. (a) The topography of individual connexons with a lateral resolution of ~1.2 nm. (b) In the presence of 0.5 mM $CaCl_2$, there is a Ca^{2+}-induced conformational change in the extracellular connexon surface. Adapted from ref. 44, Figures 3 and 4 with permission.

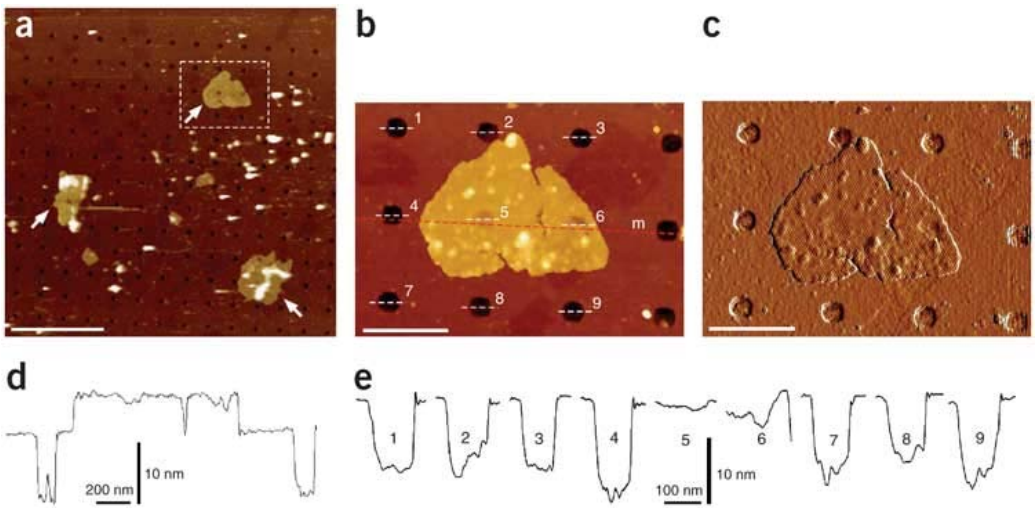

Figure 10. Membranes adsorbed on a holey silicon surface. (a) The topography of S-layer membranes. (b) Magnified topography of the S layer from a. (c) Deflection image of b. (d) Section analysis along the red line (m) in b. (e) Section analysis along the white lines (1-9) in b. Scale bars are 2 μm (a) and 500 nm (b, c). Adapted from ref. 88, Figure 1 with permission.

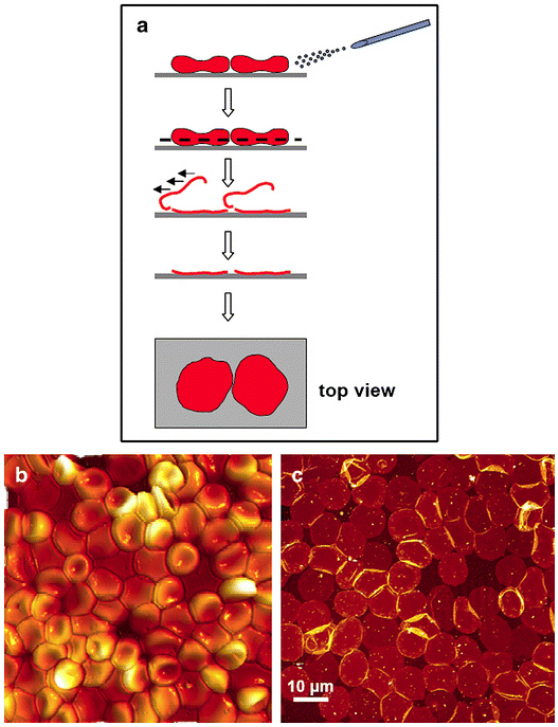

Figure 11. Membrane preparation scheme. (a) RBCs are exposed to fluid flow-imposed shear stress to open the cells. (b) AFM images of RBCs attached to poly-L-lysine-coated glass. (c) Inside-out RBC membranes spread on the glass surface after shear stress. Adapted from ref. 91, Figure 1 with permission.

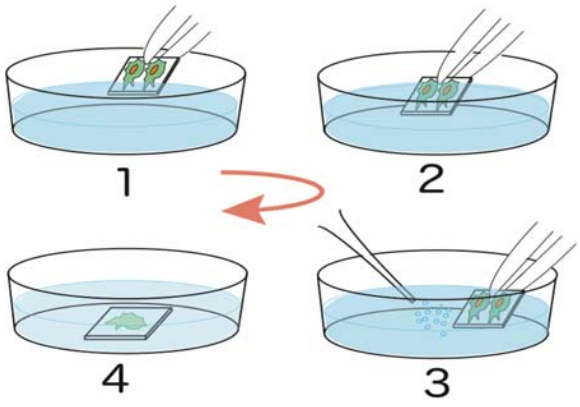

Figure 12. Scheme for unroofing cells. The cells are washed three times in hypotonic HEPES-based mammalian Ringer's solution and subsequently unroofed by ultrasonic stimulation, which removes the apical cell membrane and the cytoplasm. Adapted from ref. 95, Figure 1 with permission.

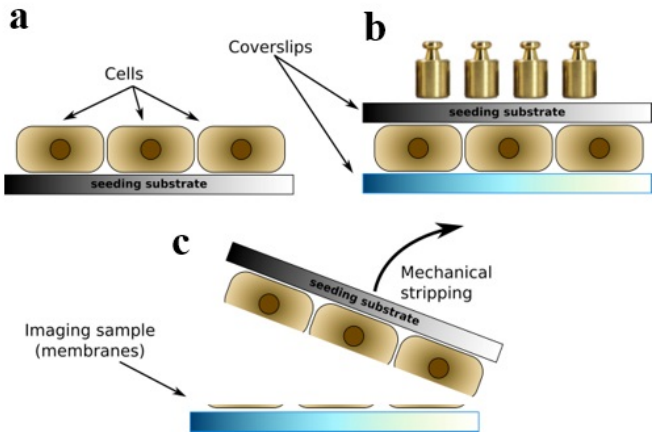

Figure 13. Scheme of the preparation of the apical cytoplasmic side of membranes. (a) Cells are cultured on a seeding substrate. (b) A coverslip covers another side of the cells, and weights are placed on the seeding substrate. (c) Stripping the seeding substrate to leave the apical membranes for imaging. Adapted from ref. 97, Figure 1 with permission.

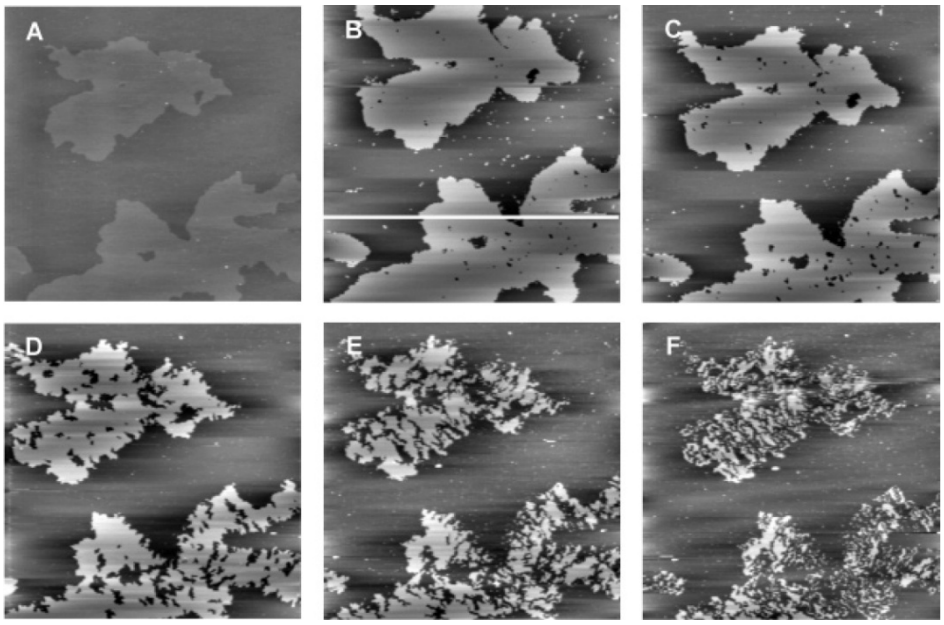

Figure 14. Supported lipid membranes treated with TX-100. (a) An AFM height image (20 × 20 μm^2) of a mixed DOPC/DPPC bilayer prior to TX-100 addition. (b-f) Serial images after the addition of 0.48 mM TX-100 for 3.5 min (b), 10 min (c), 30 min (d), 60 min (e), and 90 min (f). Adapted from ref. 108, Figures 2A-F with permission.

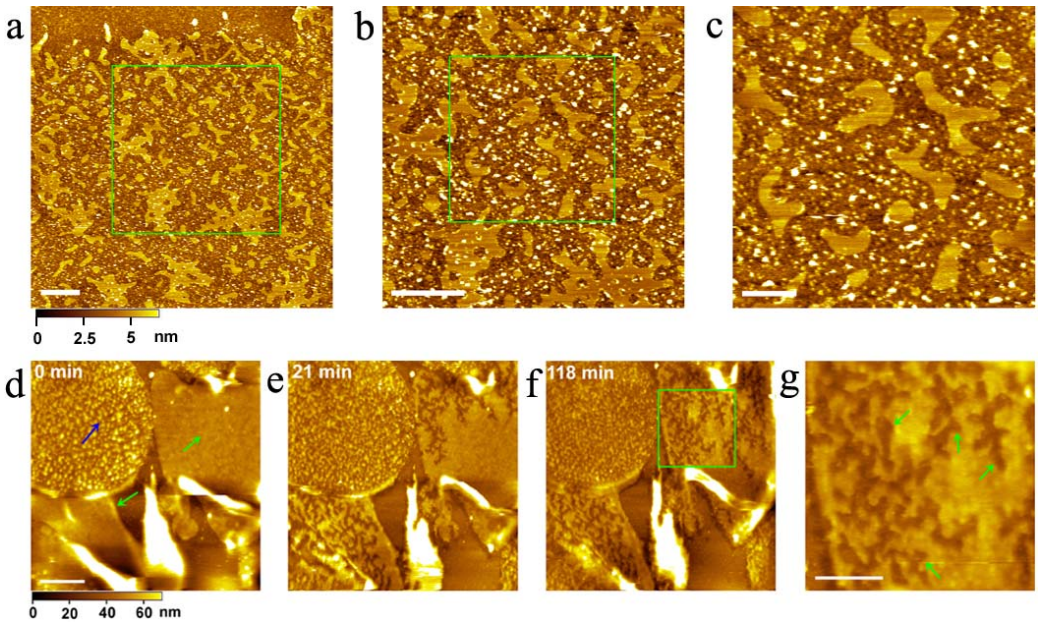

Figure 15. (a-c) DRMs from the outer leaflet membrane. (a) AFM image of DRMs. (b, c) Serial magnifications of the DRMs in (a). Scale bars are 500 nm in (a) and (b) and 200 nm in (c). (d-g) In-situ images of cell membranes treated with MβCD. (d-f) A series of images after the addition of MβCD for 0 min (d), 21 min (e), and 118 min (f). The green and blue arrows in (d) point to the outer and inner leaflets of the cell membranes, respectively. (g) Magnified image of the green square area in (f). The green arrows indicate the regions eroded by MβCD. Scale bars are 2 μm in (d) and 1 μm in (g). Figures a-c from reference 119, Figures 4A-C with permission; Figures d-g are from reference 119, Figures 2A, 2C, 2F and 2G with permission.

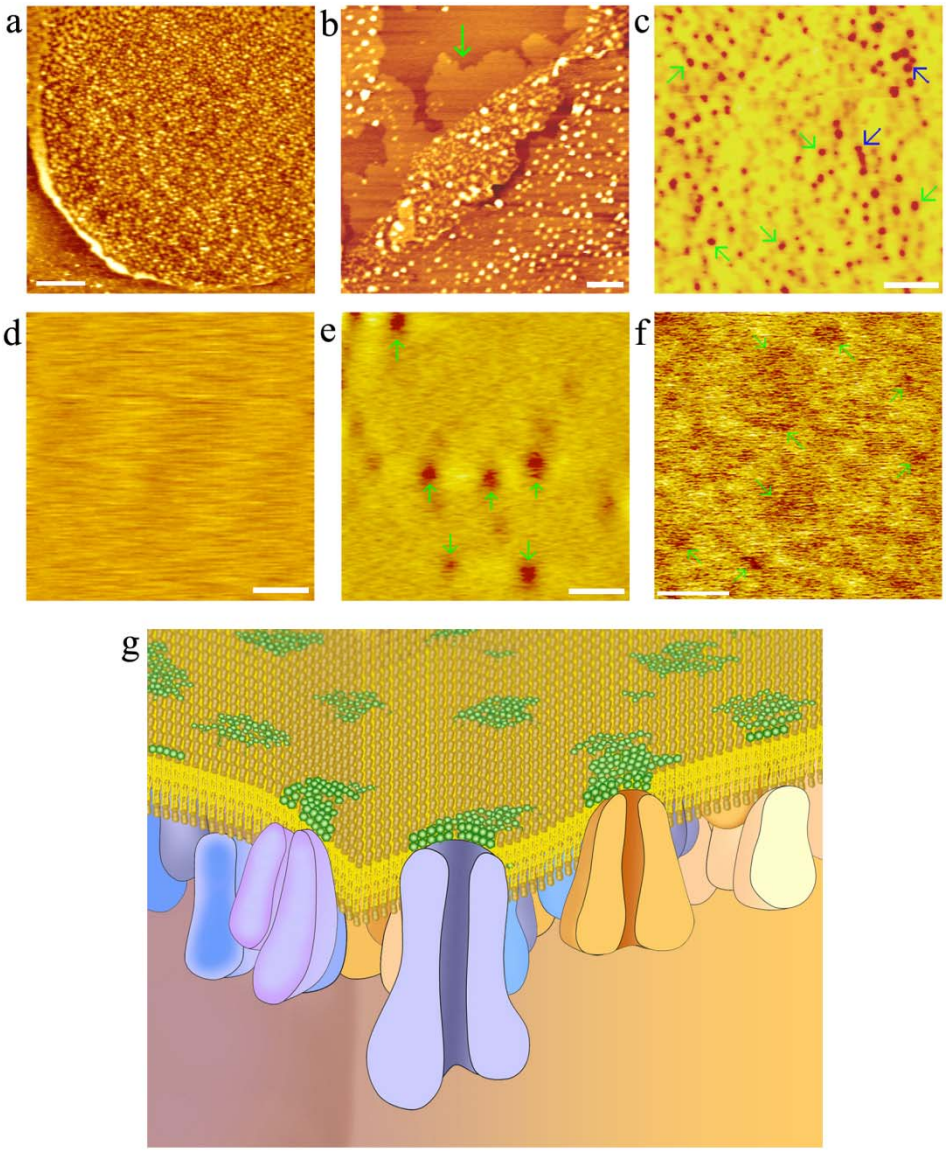

Figure 16. (a) Image of the inner membrane leaflet with dense membrane proteins. Scale bar is 1 μm. From reference 92, Figure 1D with permission. (b) Inner membrane leaflet treated by trypsin. Arrow points to the free lipid bilayer. Scale is 300 nm. From reference 92, Figure 2A with permission. (c) Recognition image of Na^+-K^+ ATPases (dark spots) in the inner leaflet of cell membranes. Red and blue arrows indicate isolated Na^+-K^+ ATPases and Na^+-K^+ ATPase aggregations, respectively. From reference 130, Figure 3B with permission. (d) Topographic image of the outer membrane scanned by a lectin (MNA-M)-functionalized AFM tip. Scale bar is 500 nm. (e) Recognition image of the outer membrane that corresponds to Figure 15d. Arrows indicate the mannose domains (dark signal) recognized by the MNA-M on the AFM tip. (f) High-resolution image of the outer membrane leaflet treated by PNGaseF. Arrows point to the presumed regions of oligosaccharide aggregations in the membrane. Scale bar is 500 nm. From reference 92, Figure 3E with permission. (g) The proposed semi-mosaic model of cell membranes. Lipids (golden) and glycans (green) are shown on the top of the layer. Membrane proteins are semi-mosaic in the lipid bilayer. From reference 92, Figure 5 with permission.

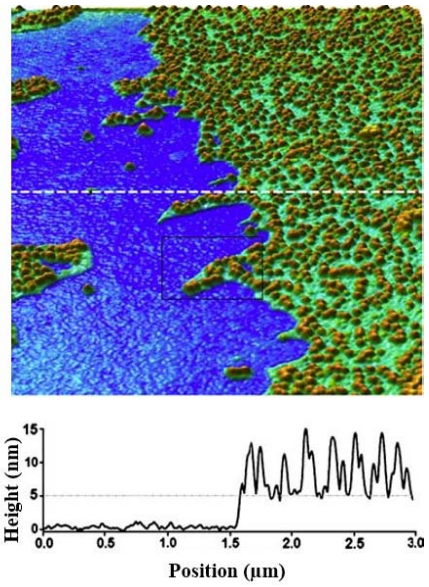

Figure 17. AFM image of South African frog oocyte membranes (cytosolic side). Poly-L-lysine-coated glass (blue), the lipid bilayer membrane (turquoise), and the membrane proteins (brown). The height profile along the broken line is presented at the bottom. From reference 91, Figure 6 with permission.

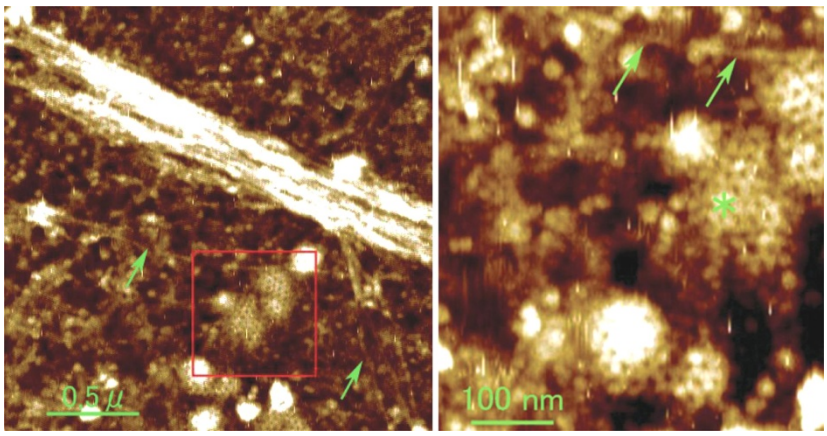

Figure 18. AFM image of clathrin coats and actin filaments at the cytoplasmic surface of the plasma membrane. The right figure shows an enlarged view of the boxed area in the left figure. Clathrin-coated pits are clearly observed in the boxed area. Arrows indicate actin filaments. From reference 95, Figure 6 with permission.

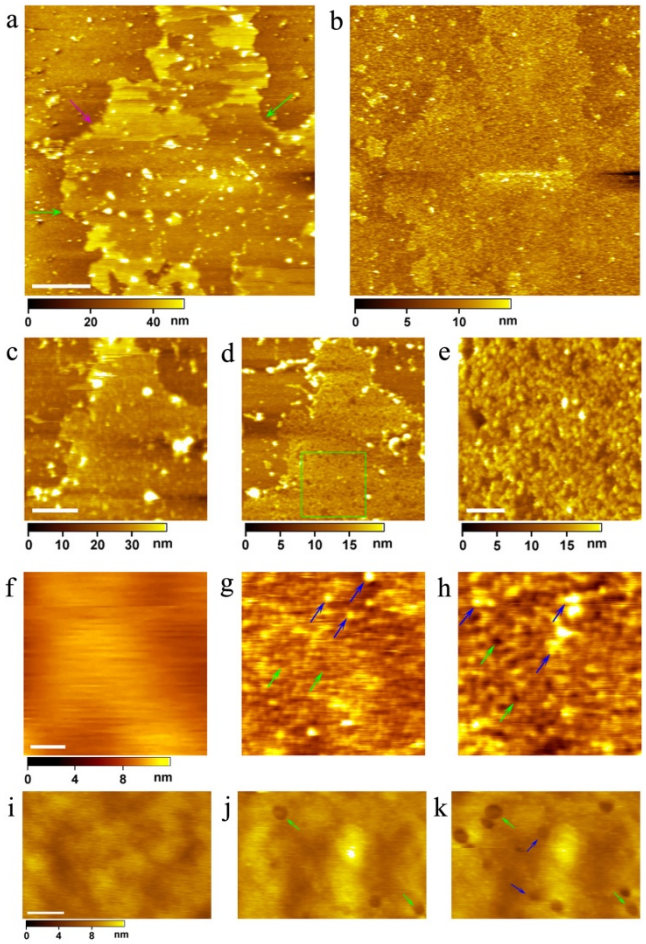

Figure 19. (a) AFM image of the cytoplasmic side of the cell membrane after digestion with trypsin for 1 h. The single and double layers of the membranes are indicated by green and pink arrows, respectively. From reference 94, Figure 5A with permission. (b) The membranes were treated in situ with 0.1% Triton X-100. The outer protein layer with about 4 nm is observed. From reference 94, Figure 5B with permission. Scale bars are 2 μm in (a-b). (c) and (d) Images of the cytoplasmic side of membranes after treatment with proteinase K and MβCD in sequence to extract lipid rafts. The heights of left membranes are about 8 nm in (c) and (d). From reference 94, Figures 5G and 5H with permission. (e) Magnified image of the green square area in (d). From reference 94, Figure 5I with permission. The scale bars are 1 μm in (c-d) and 300 nm in (e). (f) AFM topographic image of the ectoplasmic side of the cell membrane. From reference 94, Figure 2A with permission. (g and h) AFM topographic image of the ectoplasmic side of cell membranes treated with proteinase K (g) and MβCD (h) in sequence. From reference 94, Figures 2B and 2C with permission. (i) AFM topographic image of the ectoplasmic side of the cell membrane without treatment. From reference 94, Figure 2N with permission. (j and k) AFM topographic image of the ectoplasmic side of the cell membrane in situ treated with collagenase 3 (specific enzyme) and MβCD in sequence, respectively. The depths of pits (green arrows) in (j) and (k) are about 4 nm and 8 nm respectively, further confirming there is a protein layer (4 nm) on the lipid layer. From reference 94, Figures 2O and 2P with permission. Scale bars in (f-k) are 300 nm.

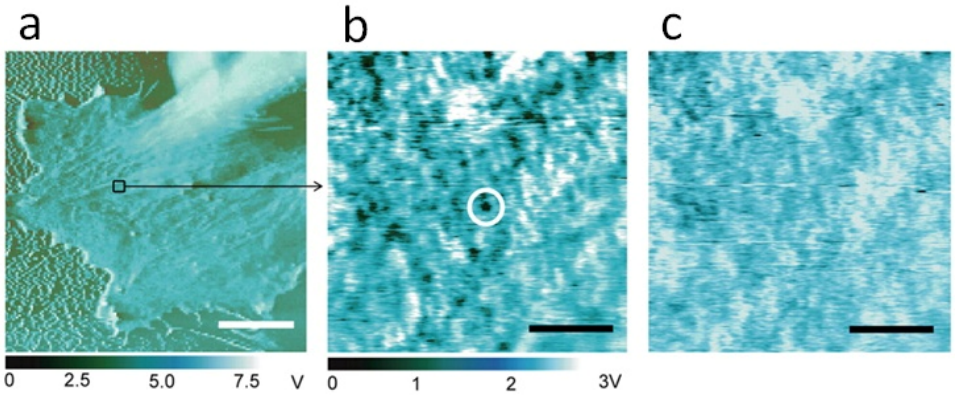

Figure 20. Imaging individual VEGFR2 receptors on fixed HUVEC surfaces using TREC. (a) Phase image of a cell. (b) The recognition image over the indicated area in "a" shows the location of VEGFR2 receptors (circled dark spots). (c) An image of the blocking induced by the addition of 5 μg/mL anti-VEGFR2 supports this binding specificity between the probe and VEGFR2. Scale bars are 10 μm for (a) and 500 nm in (b-c). From reference 54, Figures 1 A, 1B and 1D with permission.

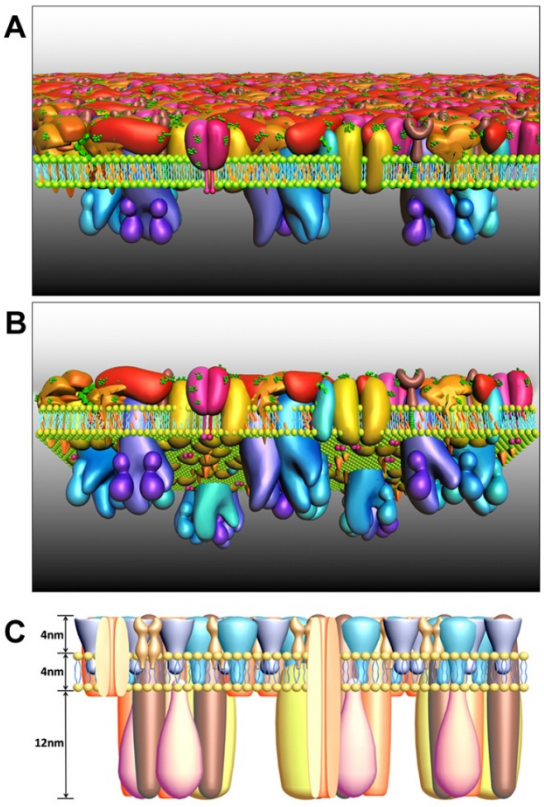

Figure 21. The proposed protein layer-lipid-protein island (PLLPI) model of the cell membrane. (a and b) The top and bottom views of the cell membrane, respectively. The proteins on the ectoplasmic side of the cell membrane form a dense protein layer, which provides a smooth feature (a); the proteins on the cytoplasmic side tend to form dispersed microdomains (b). (c) The size of the cell membrane. The total height of the cell membrane is 20 nm, and the membrane is composed of the ectoplasmic protein layer (4 nm), the lipid bilayer (4 nm) and the cytoplasmic protein layer (12 nm). From reference 94, Figure 7 with permission.

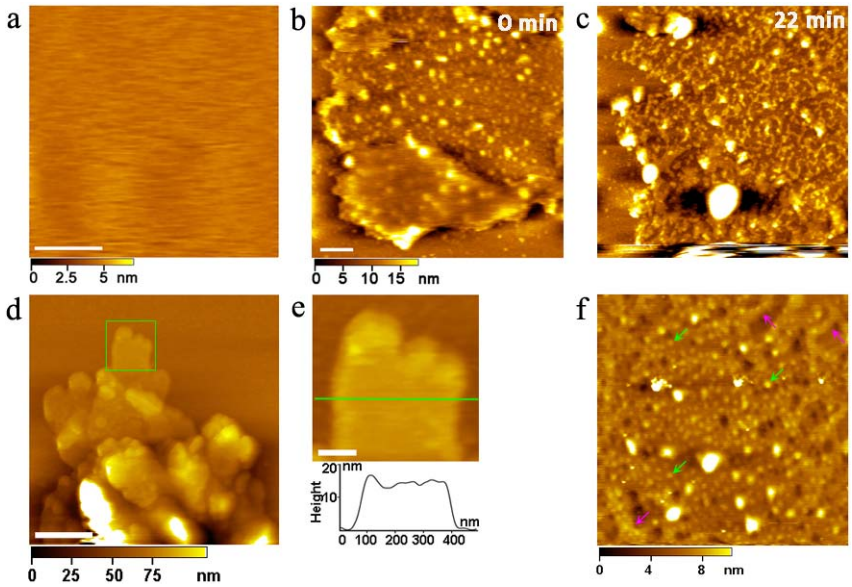

Figure 22. AFM image of individual Golgi cisternae and mitochondrial membranes. (a) Image of the outer surface of Golgi apparatus membranes. The membrane is flat without protruding proteins. The scale bar is 100 nm. From reference 140, Figure 2C with permission. (b) Image of an opened Golgi cisternae. Protein domains are located in the inner side of membranes. The scale bar is 500 nm. From reference 140, Figure 3A with permission. (c) Real-time images of a Golgi membrane treated with MβCD for 22 min. Cholesterol-enriched domains were extracted. The scale bar is 200 nm. From reference 140, Figure 4F with permission. (d) AFM topographic images of flattened mitoplasts from mitochondria subjected to a freeze-thaw treatment. The scale bar is 500 nm. From reference 141, Figure 3C with permission. (e) Higher magnification image (top) of the green square area in (d) with the cross section analysis (bottom) along the green line. The membrane is flat without protruding proteins. The scale bar is 100 nm. From reference 141, Figure 3D with permission. (f) AFM topographic images of unilamellar inner mitochondrial membranes covered by dense proteins. The scale bar is 300 nm. From reference 141, Figure 4C with permission.

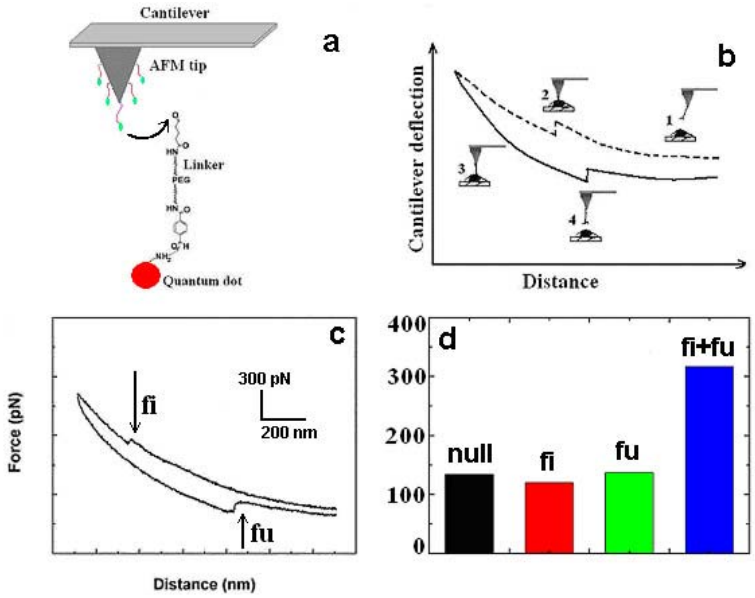

Figure 23. Force measurement of living cells during the uptake of single quantum dots. (a) Functionalization of AFM tips by QDs. (b) Diagram of a typical force curve cycle. (c) A real typical force curve that demonstrates the interactions between a single QD and a HeLa cell in DMEM at 37°C. The annotation "fi" indicates the uptake force signal; "fu" indicates the unbinding force signal. (d) Quantitative comparison of the "fi" and "fu" from more than 700 force curves (the black, red, green and blue columns represent "no peaks", "only fi peaks", "only fu peaks", and "both fi and fu peaks", respectively). From reference 156, Figures 2a-d with permission.

Table 1: Comparison of imaging techniques.

	AFM [83]	Electron microscopy [20]	Fluorescence microscopy [163]	Super-resolution microscopy [165]	Bright field microscopy
Resolution	Approximately 1 nm (XZ), 0.1 nm (Z)	0.2 nm (XY)	200 nm (XY), 500 nm (Z)	>10 nm (XY), >20 nm (Z)	250 nm (XY)
Imaging condition	Air, liquid, vacuum	Fixed sample, low temperature	Dyes or fluorescent proteins	Dyes or fluorescent proteins	Liquid
Sample preparation	Both fixing and native sample	Fixing, freezing or dyed sample	Fixed or native sample	Fixed or living sample	Living sample
Imaging mode	Versatility in the imaging modes	TEM or SEM	Inverted or confocal fluorescence microscopy	STED, PALM, STORM, SSIM	Bright field, DIC, phase
Imaging type	XYZ dimension	XY dimension	XYZ dimension	XYZ dimension	XY dimension

Table 2: Comparison of membrane thicknesses (nm).

	Red blood cells (nm) [92,133,134,135]				Nucleated Cell membranes [94]	Golgi membranes [140]	Mitochondrial membranes [141]
Thickness of lipid bilayer with outer layer	Human 2.9±0.4	Chicken 3.1±0.7	Turtle 2.5±0.5	Fish 3.5±0.6	8.0 ±0.5	3.7±1.6	7.1± 0.9
Total thickness of membranes	~10	16.5±3.6	18.5±2.4	18.2±3.0	19.5±2.8	~7.0	~10
Roughness of the ectoplasmic side	0.18	0.47±0.05	0.52±0.11	0.56±0.06	1.1±0.2	0.43±0.09	0.6±0.2
Roughness of the cytoplasmic side membrane	1.9	3.4±0.8	4.0±0.8	3.1±0.7	3.7±0.2	1.95 ±0.62	1.5±0.4

Table 3: Models of cell membranes.

Models	Methods	Method resolution	Supported by experiment	Coverage	Limitation	Dominating time
Lipid bilayer model [16]	Extraction and Langmuir methods	Macroscopic measurement	Lipid area extracted from cell membranes is double the size of cell membranes	Membrane consists of a lipid bilayer	Without the location of membrane proteins	To date
Davidson-Danielli model [19]	Surface tension measurement	Indirect measurement	Not well supported by experiments	Proteins are associated with membrane	Protein location is not accurate	Until the 1970s
Unit model [21]	Electron Microscopy (EM)	Few nanometers	Visualization of dark and bright bands by EM	Proteins are associated with membranes	Protein location is not accurate	Until the 1970s
Liquid mosaic model (LMM) [22]	EM, freeze-etching, immuno- EM	Few nanometers	Visualization of transmembrane proteins and isolated membrane proteins in the membrane	Membrane is fluidic with mosaic proteins	Lack of protein functions and interactions	To date
Lipid raft model [26]	Centrifugation, fluorescence microscopy, single-molecule tracking, AFM	Multiple scales	Isolated detergent-resistant patches, raft domains visualized by AFM	Protein exists in cholesterol-enriched domains for special functions	Lack of whole membrane structure	To date
Amended mosaic model (more mosaic proteins) [23]	Protein structure, computer simulation and EM	Multiple scales	Large functional complexes exist in membranes; proteins and lipids tend to group together	More proteins exist in membranes than in LMM membranes	Lack of whole membrane structure	To date
Semi-mosaic model [92]	AFM, in situ enzymatic method	Few nanometers	Direct imaging, in situ protein digestion, in situ detergent and MβCD treatment	Asymmetrical mosaic membrane proteins, especially for red blood cell membrane	Lack of accurate protein locations	Novel view

PLLPI model [94]	AFM, in situ enzymatic methods, super-resolution fluorescence microscopy	Few nanometers	Direct imaging, in situ protein digestion, in situ detergent and MβCD treatment	Dense and asymmetrical membrane proteins, especially for a complicated nucleated cell membrane	Lack of accurate protein locations	Novel view

Table of Content:

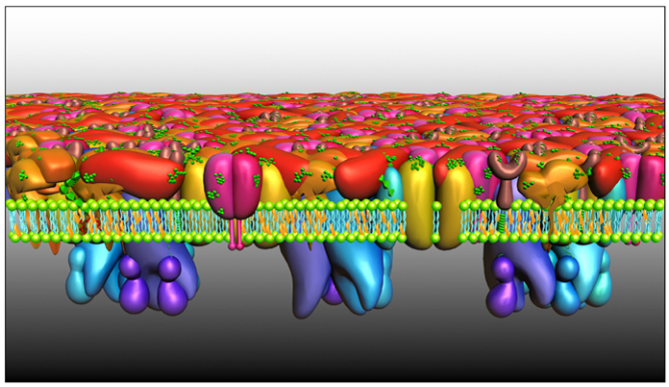

The structure and functions of cell membranes were revealed by atomic force microscopy and force spectroscopy at the molecule level.